CHALMERS

Development of Simplified Models of Doubly-Fed Induction Generators (DFIG)

A contribution towards standardized models for voltage and transient stability analysis

Master of Science Thesis

MICHAEL A. SNYDER

Department of Energy and Environment
Division of Electric Power Engineering
CHALMERS UNIVERSITY OF TECHNOLOGY
Göteborg, Sweden 2012
Report No. xxxx.xx

REPORT NO. xxxx.xx

Development of Simplified Models of Doubly-Fed Induction Generators (DFIG)

A contribution towards standardized models for voltage and transient stability analysis

MICHAEL A. SNYDER

Department of Energy and Environment
Division of Electric Power Engineering
CHALMERS UNIVERSITY OF TECHNOLOGY
Göteborg, Sweden 2012

Development of Simplified Models of Doubly-Fed Induction Generators (DFIG)
A contribution towards standardized models for voltage and transient stability analysis
MICHAEL A. SNYDER

Technical Report no. xxxx.xx
Department of Energy and Environment
Division of Electric Power Engineering
Chalmers University of Technology
SE–412 96 Göteborg
Sweden
Telephone +46 (0)31–772 1000

Cover:
Text concerning the cover illustration. In this case: Three-phase voltage.

Chalmers Bibliotek, Reproservice
Göteborg, Sweden 2012

Development of Simplified Models of Doubly-Fed Induction Generators (DFIG)
A contribution towards standardized models for voltage and transient stability analysis
MICHAEL A. SNYDER
Department of Energy and Environment
Division of Electric Power Engineering
Chalmers University of Technology

Abstract

With the increasing amounts of wind power being installed on electrical grids, the characterization of wind turbines during all operating conditions is essential for system operators to ensure security and stability for their customers. This characterization must be achieved by appropriate models of various wind turbine technologies that can accurately depict the interaction between wind turbines and the interconnected power system. Of critical importance and the focus of this thesis is the response of wind turbines during a grid fault, and specifically the wind turbines' effect on voltage and transient stability through the control of reactive power (Q) support. The DFIG wind turbine is the focus of this thesis, as it presents a more complicated model and response to transient events and thus warrants further research in the pursuit of a standardized simplified model for the purposes of voltage and transient stability analysis.

The proposed model is developed specifically for dynamic simulations in PSS/E power system simulation tool, which is a positive-sequence phasor time-domain analysis. The simulation tool is limited to a 10ms time step. Therefore there is a need to simplify the model to a level that can be depicted at this granularity but also maintain a fast simulation time for implementation in large network analyses.

A 5th order model of the DFIG wind turbine is introduced through the fundamental electrical equations that describe the machine. The control of the machine is described, including the use of an active power (P) controller, reactive power (Q) controller, a rotor speed controller, and a torque controller. A rotor voltage limitation is imposed and the effects are studied.

The stability of the DFIG with current controller is analyzed. The DFIG is recognized as a poorly damped machine with poles naturally occurring near the line frequency (50 Hz). These poorly damped poles are further evaluated through sensitivity analyses of model parameters and controller settings. A flux damping term is discussed and implemented in the DFIG detailed model. The results show successful damping for small disturbances but a high sensitivity to grid voltage dips.

The DC-chopper protection of the DFIG rotor circuit is analyzed. A simplified model for the DC-chopper protection is proposed that neglects the DC-link voltage controller and the control of the grid-side converter but instead focuses on the effects of the rotor-side converter losing controllability and entering into diode rectifier operation. Any imbalance of rotor circuit power and grid-side converter power is assumed to be effectively burned in the DC crowbar via a properly controlled DC-chopper and DC-link voltage.

The 5th order model is compared to a more detailed model developed in PSCAD. In previous research [1], the PSCAD model has been validated against field measurements for a DFIG wind turbine experiencing both a shallow and deep voltage dip. The 5th order model of this thesis shows reasonable accuracy to the PSCAD model but is not able to fully synchronize with the model. Step responses of the DFIG machine model in PSCAD was studied and compared to the 5th order DFIG machine designed in Matlab/Simulink to further analyze possible reasons for the differences in the two models.

The 5th order model is simplified into a set of algebraic equations with a Q controller, based on several assumptions. The goal of the simplified model is for implementation in PSS/E dynamic simulations with fast simulation times in complex power networks. The simplified model is compared to the detailed model and shows reasonable accuracy in depicting the general response to voltage dips for the three operating conditions (sub-synchronous, synchronous, and super-synchronous).

The machine is modeled with a fixed rotor speed and compared to the 5th order model with a variable rotor speed.

Keywords: wind turbine, simplified model, Doubly Fed Induction Generator, DFIG, power system stability, voltage stability, PSSE

Index Terms: wind turbine, simplified model, Doubly Fed Induction Generator, DFIG, power system stability, voltage stability, PSSE

Acknowledgements

This work has been carried out at the Department of Energy and Environment at Chalmers University of Technology. A sincere and special thanks to Peiyuan Chen, as his dedication and passion to teach created an environment for success and an enjoyable learning atmosphere. A special thanks to Massimo Bongiorno for his guidance and focus on understanding the fundamental concepts of this thesis, and for his dedication to repetitive teaching with patience. Thank you to Stefan Lundberg for his never-ending patience and openness to unscheduled walk-ins, for his explanations around control theory, DFIG theory, and Matlab/Simulink model development, and of course for the unplanned and informal adoption of me as his masters thesis student.

A heart felt thank you to my wife, Mandy, for her patience and her never ending support throughout my time at Chalmers. A special smile and thank you to my son, Elliot, who gives me inspiration and excitement every day. Although you cannot read this yet, someday you will, and hopefully you will think it is pretty cool.

Michael A. Snyder
Göteborg, Sweden, 2012

Contents

Chapter 1

Introduction

1.1 Background and Motivation

Wind power generation has continued to increase worldwide, with the latest annual report stating installed wind power worldwide of 239 GW at 2011 year's end, which is enough to cover 3% of the world's electricity demand. Worldwide growth continues at approximately 24% per year [2]. With this increase in wind power generation, their penetration levels and influence on utility grids has grown as well. The penetration has become substantially high in particular countries, including Denmark (22%), Spain (15.4%), Portugal (21%), Ireland (10.1%), and Germany (6%). Additionally there were four German states that met over 40% of their energy demands via wind power [3]. These figures represent annual energy production as a function of total electricity demand, so actual *peak* penetration could be substantially higher than these figures.

As the penetration of wind power increases, so too does the importance of ensuring that the wind power generation does not adversely affect the power quality, security, and reliability of each power system network, during both steady-state operation and under a contingency scenario. Therefore, traditional forms of modeling wind turbines as either distributed small generators or as negative loads are no longer adequate. These traditional representations must be updated to properly model wind turbines interaction with the grid in order to properly predict security or reliability issues.

Coupled with this realization of increasing grid penetration is the action of many grid operators to introduce more demanding grid codes for wind power interconnections. The requirements for the dynamic performance of grid connected wind turbines are mainly centered around the wind turbine's ability to stay on-line during a voltage dip, a term referred to as fault ride-through or FRT. FRT requirements can be coupled with requirements for reactive power support to assist with voltage stability. Wind turbine manufacturers must incorporate this fault ride-through and reactive power support functionality

into their products.

This thesis will analyze the behavior of Doubly-Fed Induction Generators (DFIG) used with wind turbines to capture wind energy and transfer it to the grid. The DFIG has two connections to the grid - a direct connection to the main terminals of the stator windings, and a connection to the wound rotor windings via back-to-back voltage source converters (VSCs). The DFIGs response in the presence of grid dynamics, for example a short circuit causing a voltage drop or varying loads and generation causing voltage and frequency deviations, is of primary interest in this research. The DFIG has a unique response due to these two grid connections - the rotor can be controlled quickly with the VSC, while the stator is directly coupled to the grid and therefore directly affected by voltage fluctuations of the grid. This unique arrangement, coupled with the popularity of the DFIGs use in wind technology, makes the DFIG a critical machine to properly understand and model in the context of grid stability analysis, as well as utility feasibility and planning studies. Utilities must be able to properly model both new and existing wind turbines in order to predict grid stability and security, a key to ensuring the continued growth and penetration levels of wind energy.

Previous research in the development of a simplified model has made certain assumptions and simplifications. With each simplification, the model is limited and its accuracy decreased. The acceptability of this compromise is a function of the expected use and application of the model. Therefore it is essential in this research to understand the purpose of previous simplifications, state the validity of these simplifications, and determine what simplifications are required or not required in order to properly model the DFIG for the purposes of grid stability analysis.

1.2 Description of Wind Turbine Generator Types

A fundamental concept in understanding wind technology is wind energy capture. Wind holds in it a discrete amount of power at any given point in time, dependent in large part on the wind speed. As wind speed can vary greatly, wind turbines must be capable of operating over a wide wind speed range. The wind turbine can operate in one of two ways. The first is to have a relatively fixed rotational speed, in which an increase in wind speed can slightly increase the rotor speed above the synchronous speed and thus varying the slip. This is based purely on the torque-speed relationship of an induction machine. The wind turbine can also operate as a variable-speed machine, varying the rotor speed based on the wind velocity. A speed controller is used to vary the pitch of the wind turbine blades during high wind speeds to reduce the power intake and protect the wind turbine, in which case the rotor speed is also controlled in order to optimize the ratio of wind speed to rotor speed. The goal in varying the pitch is to maximize efficiency by optimizing a

term called the *tip-speed ratio*. The tip-speed ratio (λ) is defined as:

$$\lambda = \frac{v_{tip}}{v_{wind}} \tag{1.1}$$

where v_{tip} is the velocity of the blade tip and v_{wind} is the wind velocity. The tip speed velocity can be calculated from:

$$v_{tip} = \Omega \times r \tag{1.2}$$

where Ω is the mechanical speed of the wind turbine and r is the radius of the circle of rotation, in this case the length of the wind turbine blade. From here it can be seen that the ability to maximize the aerodynamic efficiency of energy capture, is directly related to the ability to vary the rotational speed. There are several configurations for variable speed wind turbines that allow for the generator's rotor to operate at a variable rotational speed.

The various configurations for fixed and variable speed wind turbine generators can be broken down into four main types to be described in the following sections.

1. Fixed Speed Wind Turbine (FSWT) with induction generator
2. Variable Speed Wind Turbine (VSWT) with variable rotor resistance
3. VSWT with Doubly-Fed Induction Generator (DFIG)
4. VSWT with Full-Power Converter (FPC)

There are common components with each of the configurations as seen in the figures for each. A gear box is used in between the wind turbine and generator to convert the lower rotational speed of the turbine to a higher rotational speed for the generator rotor. Also, a step-up transformer is used to connect the wind turbine generator to the grid, transforming the voltage up as needed to connect to the distribution or transmission system [4] [5].

1.2.1 Fixed Speed Wind Turbine

Figure 1.1 shows the basic configuration for the fixed-speed wind turbine connected to the grid via an induction generator. The stator terminals are connected directly to the grid, and thus the generator rotor rotates at a fixed speed based on the grid frequency and number of pole pairs of the machine. The turbine rotor will therefore also rotate at a fixed speed, dependent on the rotor speed and also the turns ratio of the gear box. The induction machine by its nature acts to absorb reactive power (as implied by the name "induction"), therefore capacitor banks are used to provide this reactive power locally and minimize the reactive power drawn from the grid. Since the rotor speed is for the most part fixed, wind power variations will result in a power delivery that fluctuates and adversely affects the power quality of the grid [5].

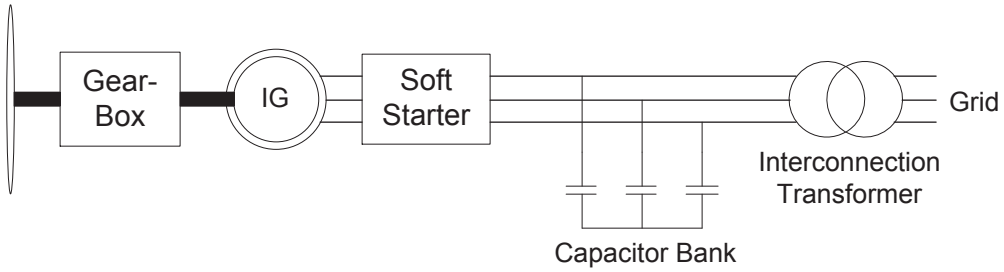

Figure 1.1: Fixed Speed Wind Turbine

1.2.2 Variable Speed Wind Turbine with Variable Rotor Resistance

With this configuration, the rotor resistance can be varied by connecting a resistance to the rotor terminals via slip rings. The rotor speed can then be controlled by varying this resistance, thus making this arrangement a variable speed wind turbine (VSWT). Capacitor banks are still required to compensate for the reactive power consumption. While this does provide some controllability to the rotor speed, this arrangement only allows for rotor speeds *higher* than synchronous speed, not lower. This arrangement diverts all excess energy through the resistors - an unnecessary waste of energy as will be shown in the description of the DFIG [5].

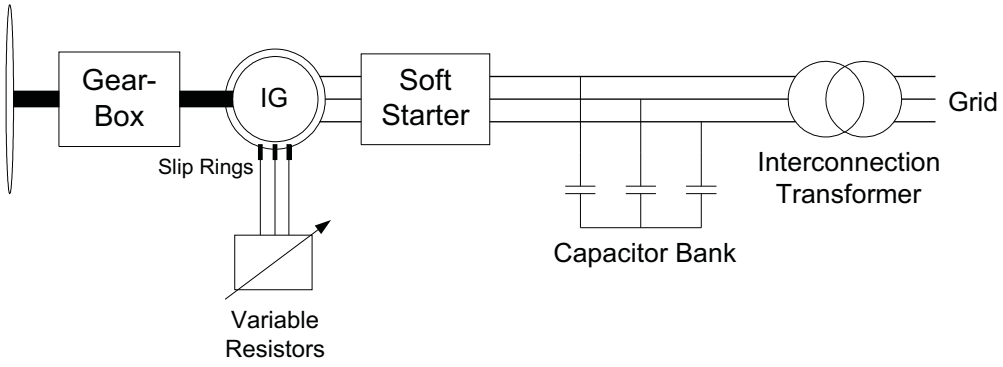

Figure 1.2: Variable Speed Wind Turbine with variable rotor resistance

1.2.3 Variable Speed Wind Turbine with Doubly Fed Induction Generator

In this configuration, the stator terminals are directly connected to the grid, while the rotor windings are connected via slip rings to a three-phase voltage source converter. Therefore, both the stator and the rotor are connected to the grid, thus giving the name ”doubly-fed” generator. As in the previous configurations, a step-up transformer is used to increase the stator and rotor voltage to the grid voltage, in this case a three-winding transformer is used in order to couple both the stator and rotor with the grid.

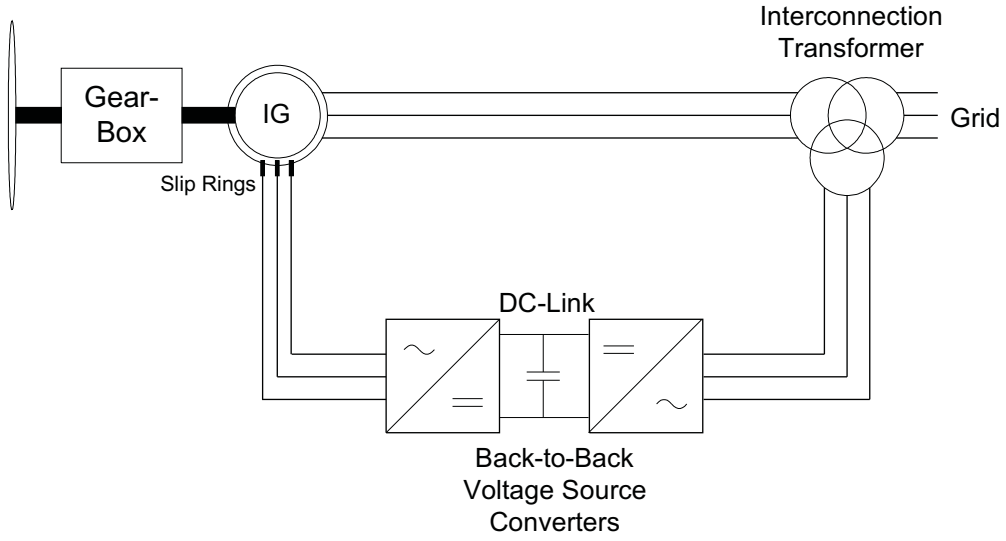

Figure 1.3: Variable Speed Wind Turbine with Doubly Fed Induction Generator

There are several advantages to the DFIG setup. The controllability of the rotor is increased with the converters, allowing for control of the rotor speed at around +/- 30% of synchronous speed, as well as reactive power control. The controllability range around synchronous speed depends on the sizing of the converters, as they must be sized to handle the slip power in the rotor circuit. Compared to the configuration with variable rotor resistance, the energy can be recovered and exported to the grid. Since the converters are connected to the rotor, they must only handle the slip power, which is only a fraction of the total rated power ($\sim$30%). This allows for a configuration that offers a variable speed wind turbine, with a converter that is smaller, cheaper, and with less losses than a system with a converter rated for full power (see Full Power Converter configuration in following section) [5].

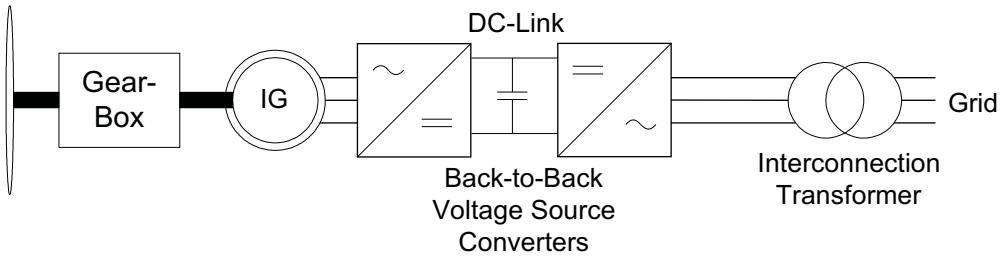

Figure 1.4: Variable Speed Wind Turbine with Full Power Converter

1.2.4 Variable Speed Wind Turbine with Full Power Converter (FPC)

Figure 1.4 represents a VSWT with a full power converter. With this configuration, back-to-back VSCs are connected directly to the stator terminals of the generator, which can be either an induction generator or a synchronous generator. All of the power must flow from the generator through the converters to the grid, requiring the converters to be rated for the full power capacity of the generator. The power rating is one of the limiting factors of this arrangement as it requires larger converters and components. As shown in Figure 1.4, the FPC WT is connected to the grid through a step-up transformer. An AC filter is also commonly included prior to the point of common coupling, not shown in the figure here.

With the FPC, the machine-side converter can be used to give full controllability of the rotor speed, making this system very flexible. In addition, the Voltage-Source Converter used in this application is commonly used in other power system applications (such as HVDC converters and STATCOMs), which makes the control and operation a well-developed and robust methodology [5].

1.3 Problem Formulation

The overall aim of this research is to *develop and verify* a simplified model of the DFIG for implementation in PSS/E that is able to properly represent the DFIG's response in the context of transient stability and short term voltage stability. The simplified model will be used in this research to study the ability of the DFIG to provide grid support through control of active power and reactive power.

1.3.1 Objectives and Tasks

In order to meet the aim of this research, the following objectives and associated tasks were set forth.

1. Develop a *detailed* model of the DFIG:
   - Define the meaning of *detailed* in the context of this research.
   - Present the equations that describe the machine.
   - Design different control algorithms.
   - Build the state-space model in MATLAB.
   - State any assumptions or simplifications. This detailed model will still represent the VSC as a controllable DC voltage source, and will not include converter switching dynamics.
   - Study the effect of the DC-chopper and implement a model in Matlab.
2. Identify current research and efforts in the development of simplified DFIG models for grid stability analysis:
   - State the simplifications made on previous research efforts.
   - State why these simplifications were made, and the impact on the simulation results.
   - State the limitations of these simplifications (what problems cannot be solved properly with these assumptions).
3. Study the accuracy of the model:
   - Compare to a more detailed model of the DFIG which includes converter switching. For this point, a pre-built PSCAD model of the DFIG system will be utilized that has been validated against a field measured DFIG response to voltage dips.
   - Qualitative analysis to determine smallest time-step/frequency at which both models are in agreement. For example, determine if the PSCAD model simulation shows a significant divergence from the MATLAB model for different time-steps in the simulation, and determine if this is acceptable for the purposes of the system level analysis that will be required of this model.
4. Derive a simplified model from the detailed model created in MATLAB:
   - Identify the purpose of the simplified model (implement in PSS/E for grid stability analysis through the delivery of P and Q).
   - State what simplifications can be made in order to keep this goal/objective valid in the model.

- State how previous simplifications are/were not sufficient.
- Develop simplified models using one simplification at a time, clearly stating each model simplification with purpose.
- Develop final simplified model as a set of algebraic equations to describe the machine, with an active and reactive power controller.

5. Compare simplified models to the detailed model:
   - Compare each simplified model to the previous model iteration, starting with the detailed model (created in MATLAB in task 1).
   - Run simulations to various voltage dips and operating points to study model accuracy.
   - Develop conclusions regarding the impact of various model simplifications to the accuracy and response of the model to various voltage dips and under various operating points.
   - Develop conclusions on the accuracy of the final simplified model with respect to the 5th order detailed machine model. State the conditions of use the model is valid for power system analyses, and the conditions under which it may not be valid.

1.3.2 Methods

The following methods were used in the research to accomplish the previously described objectives and tasks.

- Power system theories and mathematical methods for the derivation of the machine model equations.
- State-space implementation and Matlab for modeling of differential equations.
- Internal Model Control (IMC) for design of controller.
- Verification of model against PSCAD model that is validated with field measurements.

Chapter 2

Grid Codes for Grid Integration of Wind Farms

2.1 Dynamic requirements for grid integration of wind farms

Wind power generation growth has reached a level where their impact to the overall power system cannot be neglected. Many system operators have established requirements for the interconnection of wind farms to protect grid stability and reliability. These requirements can be summarized into the following categories [6]:

- **Operating Voltage and Frequency Range**. Utilities typically require wind farms to stay connected within specific voltage and frequency windows, with specific times associated with different voltage and frequency deviations from nominal. For example, the wind farm will be expected to operate continuously for a certain window around nominal voltage and frequency, but the requirement to stay connected decreases the further the voltage and frequency deviate from nominal. This requirement is typically represented in a table or chart format.
- **Ramp Rate Control**. This requirement is related to the speed at which the wind farm's active power increases or decreases. Utilities require that a wind farm not ramp up or ramp down too quickly to minimize the impact of fast active power fluctuations to the stability of the power system. This requirement is stated in terms of MW per minute or MW per second.
- **Voltage and Reactive Power Support**. Reactive power requirements vary in implementation across the various grid codes. Some can be in the form of power factor control, while others require reactive power transfer as a function of the voltage at the point of interconnection.

- **Fault Ride-Through (FRT)**. Fault ride-through is an important grid code requirement that requires a wind farm to stay connected to the grid during a voltage dip. The severity of the voltage dip that it must ”ride through” and the duration it must ride through vary across grid codes and are typically represented in a chart format.

The two requirements under study in this thesis are the reactive power support and the fault ride through, as these have the greatest impact on voltage and transient stability.

2.2 E.ON Grid Code Requirements

E.ON grid code requirements are used in this thesis as an example of reactive power support for voltage stability purposes. E.ON Netz is a transmission system operator (TSO), which operates in Europe. They have developed formal requirements for the interconnection of wind plants, both onshore and offshore. Their requirements are commonly used as examples due to the clear graphical format in which they present, for example, reactive power support requirements during grid faults.

Figure 2.1 represents the E.ON grid code requirement for reactive power support during grid faults. The chart shows how the reactive power support is dependent on the severity of the voltage dip. There is a dead band between 0.9 and 1.1 per unit, meaning reactive power support does not begin until a voltage dip over 10% occurs (this dead band is decreased to 5% for offshore wind farms). The reactive current requirement is static and is scaled based on the slope of 2 p.u., which represents the amount of current injection per the amount of voltage lost. The slope of 2 equates to the wind farm providing 100% of its available current for reactive power support during a voltage dip of 0.5 p.u.. For more severe voltage dips, the generator continues to provide the maximum amount of reactive power support. This requirement states that the wind farm shall provide the same amount of reactive current support for a time period of 500 ms after the voltage dip returns within the dead band range.

The detailed and simplified models of this thesis will implement the E.ON grid code requirements for reactive power support during the grid faults.

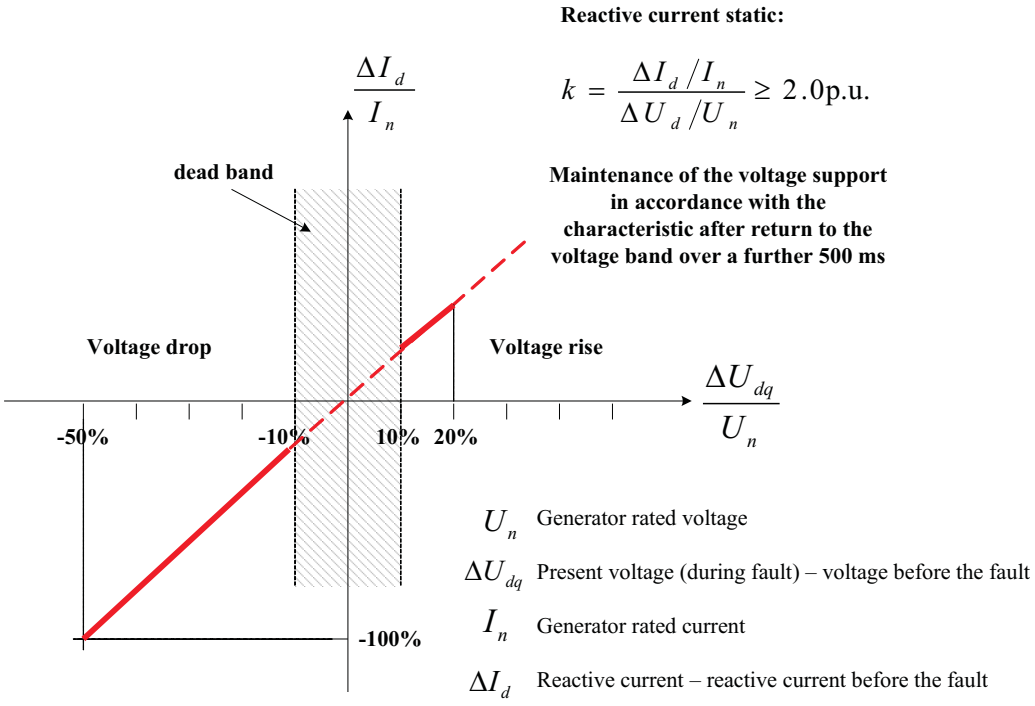

Figure 2.1: E.ON grid code requirement for reactive current support during grid faults

Chapter 3

DFIG Detailed Model

The terms ”detailed” and ”simplified” are used to describe the various machine models in this research. There are several degrees of both ”detailed” and ”simplified” that can be used to describe any model - the main point being any model is still a model and not a real turbine or generator. In order to analyze any phenomenon, simplifications must be made to represent it, and these simplifications must be clearly understood.

In the context of this research, the detailed model will be derived from the equivalent electrical circuit of the DFIG. It is detailed in the sense that the model is derived directly from the governing electrical equations, resulting in a 5th order system that includes the electrical dynamics from the rotor flux, stator flux, and rotor speed. However, this detailed model neglects several factors that influence the behavior of an actual wind turbine with DFIG configuration (which many would argue makes this model simplified!). The following assumptions have been made for this detailed model:

- pitch control of the wind turbine is not activated,
- tower shadowing effects based on the spacing of the wind turbines in a wind farm are not considered,
- mass transfer dynamics are neglected (the entire assembly from wind turbine to generator is considered as a single rigid mass),
- perfect estimation of grid voltage angle,
- PWM switching of the converters is neglected,
- the machine is symmetrical,
- losses from friction and windage are neglected,
- the skin effect is neglected,

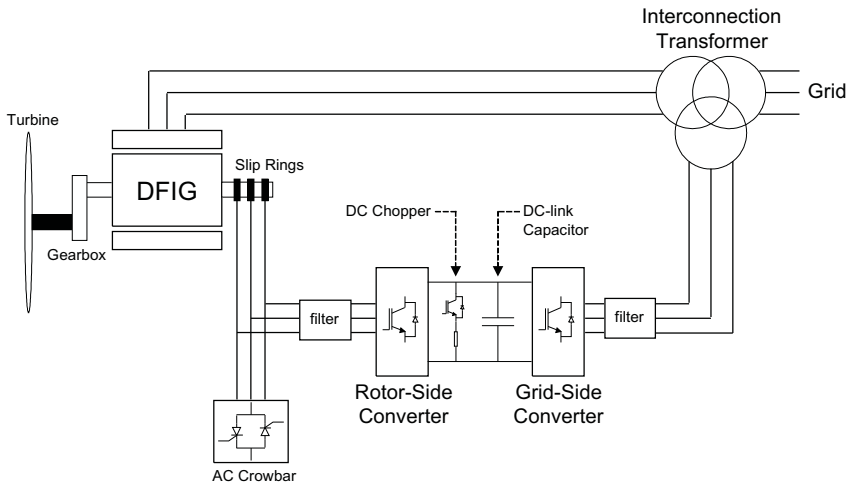

Figure 3.1: Components of the Doubly Fed Induction Generator

- iron losses are neglected,
- magnetic saturation is neglected.

From here, the detailed model will be analyzed and compared against a ”more detailed” model (to be elaborated in the section *Validation of 5th Order Model against PSCAD Detailed Model*). The model will then be simplified for implementation into PSS/E grid stability studies.

3.1 The Doubly Fed Induction Generator (DFIG)

This section introduces the basic operation and functionality of a Doubly-Fed Induction Generator (DFIG). The DFIG is an attractive and popular option for large wind turbines (multi-MW) due to its flexibility in variable speed range and the lower cost of the power converters. Figure 3.1 illustrates the major components of the DFIG to be discussed in this section.

In the DFIG configuration, the generator rotor operates at a variable speed in order to optimize the tip-speed ratio λ. The generator rotor speed is controlled to operate within a variable speed range centered around the generator synchronous speed. Therefore the generator system operates in both a sub-synchronous and super-synchronous mode, typically between +/- 30% of synchronous speed. The rotor is controlled by a 3-phase converter connected to the wound rotor windings via slip rings. The stator is connected directly to the grid. Back to back VSCs are included in the rotor circuit. The converters must only

handle the rotor power (only a fraction of the total generator power), which is typically around 30% of rated power.

This section will describe the basic topology and operation of the DFIG, and will cover an explanation of torque production, variable speed control and impacts to power flow in the machine, power converter functionality, and the AC and DC crowbar protection features.

3.1.1 Torque production in the DFIG

The DFIG consists of stator windings connected directly to the grid, and wound rotor windings connected to a power converter. The stator windings are therefore energized by the grid to create the stator magnetic field. The rotor windings are energized by the converter to establish the rotor magnetic field. Torque is created by the interaction of the rotor magnetic field with the stator magnetic field. The magnitude of the generated torque is dependent on both the strength of the two magnetic fields, and the angular displacement between the two. For example, if the magnetic fields are completely aligned, as in two bar magnets with north and south poles aligned, there is no torque generated. However if the two magnets are placed orthogonal to each other, with the north and south poles 90 degrees displaced, the attraction will be the strongest and thus the generated torque the greatest. Mathematically this can be described as the vector product between the stator and rotor fields [7].

As the stator is connected directly to the grid, the stator field is a function of the grid voltage, with a rotation based on the grid frequency and coinciding with the synchronous speed. The grid voltage can be assumed to be more or less constant (during steady state operation), and therefore the stator flux can be considered constant. The rotor flux is dependent on the rotor current, which is controlled directly by the power converter. Therefore, the torque production in the DFIG can be directly controlled by control of the rotor current magnitude and angular position relative to the stator flux. This is done by calculation of the angular position and magnitude of the stator flux by monitoring the applied stator voltage (which in this case is the grid voltage magnitude and phase), and controlling the rotor currents such that they are normal to the stator flux, at the magnitude required to generate the needed torque [7].

3.1.2 Rotor side converter (RSC)

The rotor side converter (RSC) is used to control the torque production of the DFIG through direct control of the rotor currents. The RSC does this by applying a voltage to the rotor windings that corresponds to the desired current. The RSC will operate at

varying frequencies corresponding to the variable rotor speed requirements based on the wind speed.

The rotor side converter can use either a torque controller, speed controller, or active power controller to regulate the output power of the DFIG. This output power is controlled to follow the wind turbine's power-speed characteristic curve. Essentially, any given wind speed corresponds to an amount of available power that can be extracted from the wind. In order to extract this power most efficiently, the optimal tip-speed ratio must be kept before rated power is reached, corresponding to a different rotor speed for each power level. This calculation is done for any given wind turbine, resulting in a unique power-speed characteristic curve. The actual output power from the generator, plus all power losses, is compared to this reference power from the power-speed curve. Typically a Proportional-Integral (PI) controller is used to control the torque, speed, or power to its reference value. Whichever controller is used, the output of the controller is the reference rotor current required to generate the desired torque or power, or to obtain the desired speed. An inner PI control loop is then used to control the rotor current error to its reference value, with the rotor voltage reference as the controller output [7].

The rotor current can also be used to control the reactive power production of the DFIG. The details of both the torque and reactive power control will be elucidated in the section *Control of the DFIG Machine*.

3.1.3 Grid side converter (GSC)

The grid side converter is used to regulate the voltage of the DC link between the two converters. The GSC contains on outer loop control that controls the DC-link voltage, attempting to control it to nominal value. An inner PI control loop controls the GSC current. Commonly the GSC acts to set $Q_{gc} = 0$ and maximize active power output. As the GSC is connected directly to the grid, it must output power at a fixed frequency corresponding to the grid frequency [5].

3.1.4 Power flow in the DFIG

There are multiple aspects to the power flow that must be understood to fully grasp the DFIG operation. The first to be described here is the rotor circuit. In the rotor circuit, active power flows in one direction, either to the rotor or from the rotor, thereby either absorbing or injecting active power to the grid. In either case, the active power flows in only one direction through both converters. The converter arrangement allows for a variable frequency (associated with the variable rotor speed) to maximize active power extraction. As the two converters are decoupled via the DC-link, the connection to the

grid can be maintained at the grid frequency and the voltage controlled to synchronize with the grid.

The basis for injecting or absorbing active power is the varying operation of the DFIG when it goes from sub-synchronous speed to super-synchronous speed. Active power flows as a function of slip. Recall that the synchronous speed is the speed corresponding to the grid frequency, which is also the speed at which the stator flux rotates. At synchronous speed w_s (when the required rotor speed for a given power level is exactly equal to w_s), the magnetic field of the rotor rotates at the same speed as the stator magnetic field. The DFIG then essentially operates as a synchronous machine with DC current in the rotor windings, meaning no active power will be generated in the rotor windings and therefore all active power from the DFIG machine will flow from the stator to the grid.

When the wind speed increases, the speed of the rotor must change in order to optimize the efficiency of the aerodynamic system (as described previously with the tip-speed ratio λ). Therefore the rotor speed increases above synchronous speed, resulting in a negative slip and super-synchronous operation. In this operation, power flows to the grid from both the stator windings and the rotor windings. As the wind speed decreases, rotor speed decreases, and the machine operates in sub-synchronous mode, with a positive slip. Under these circumstances, the rotor must absorb active power from the grid, essentially borrowing power for rotor winding excitation.

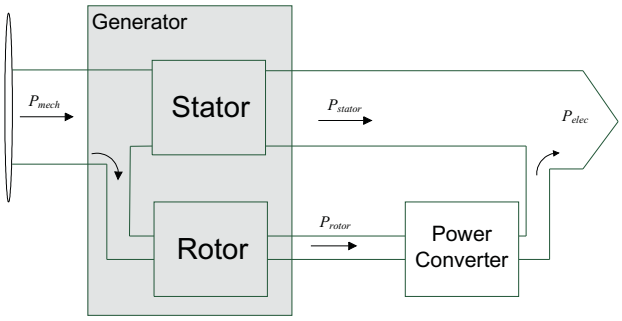

Figure 3.2: Active power flow in the DFIG during super-synchronous operation

During steady-state operation and assuming the current limits of the converter have not been reached, the power output from the DFIG machine to the grid is the sum of both stator and rotor power (P_s, P_r). However, realizing that the rotor power must then go through the Grid Side Converter before reaching the grid, the total delivered power is calculated using P_{gc} in lieu of P_r. The total power output must be equal to the total power in, calculated as the mechanical power P_m delivered to the wind turbine based on a given wind speed. Therefore, it is possible to maximize the efficiency of the power extracted from the wind by measuring the total power output, and using this information to vary the rotor speed to correspond to the input mechanical power [6].

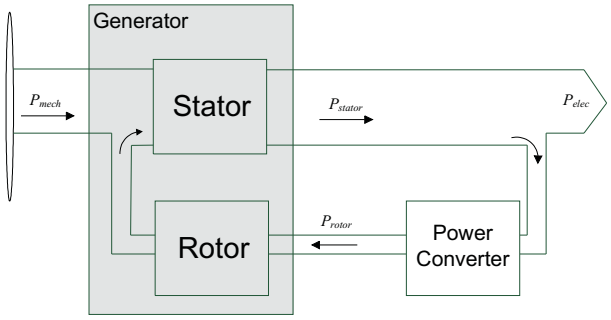

Figure 3.3: Active power flow in the DFIG during sub-synchronous operation

3.1.5 DC-link chopper / DC crowbar

A braking resistor is provided in the dc-link bus as a form of protection to dissipate excess energy during a grid fault. The resistor is connected to the dc-link bus in series with an IGBT, and is referred to as either the dc-link chopper or the dc crowbar. The IGBT can control the amount of energy burned in the resistor, with the resistor (or set of parallel resistors), sized to handle a specific amount of energy during a grid fault. The larger the fault that is desirable to ride through, the larger the physical size of the resistor or resistors must be. This design decision can be a function of utility requirements for fault ride through, as the energy dissipation during a fault is a function of the voltage dip magnitude and fault duration [7] [6].

3.1.6 AC Crowbar

An AC crowbar is implemented on the rotor side of the RSC, which acts to bypass the RSC by applying a short-circuit to the rotor terminals. This acts to protect the RSC from overcurrents as well as to protect the DC-link from overvoltages. The crowbar can be constructed by the use of either anti-parallel thryristors connected to external resistances on the rotor phases, or a diode rectifier bridge in series with a single external resistance. When using a diode rectifier bridge, a single thyristor must still be used to control the activation and deactivation of the crowbar.

The crowbar is an important aspect in not only the protection of the converter components, but in understanding the behavior of the DFIG machine during grid faults. As described, the crowbar acts to protect the rotor-side converter from overcurrents and protect the DC-link from overvoltages. Therefore, the behavior of both the rotor current and rotor voltage, as well as the typical setpoints for overcurrent and overvoltage protection, must be understood in order to adequately represent a *detailed* DFIG model. The amount of detail in the crowbar action that is carried through to any *simplified* models is an im-

portant question that is studied in later sections with the derivation of the DFIG simplified model.

In [6], several common parameters are listed for crowbar activation. For dc-link overvoltage protection, a common setting is at 12% above nominal voltage. For overcurrent protection, the converter IGBTs can typically handle twice the nominal current for a short duration. Therefore a common overcurrent protection for the converter is set near 1.8 pu. These parameters are specific to each converter manufacturer, but may be considered reasonable assumptions when developing a generic DFIG model.

One interesting aspect of the crowbar action that impacts the DFIG response to grid faults is the speed at which the crowbar can switch on to dissipate energy and switch off to return to normal operation mode. A thyristor can only disconnect the current at a zero crossing, which, coupled with the issue of fault currents containing dc-components, causes a slight delay on the order of tens of ms [6]. An active crowbar utilizing an IGBT can be used to force commutation of the rotor current and operate more quickly than the thyristor.

3.2 5th Order Machine Model

The first model of the DFIG that will be developed and analyzed in this thesis is the 5th order transient model. The model is developed from the basic electrical circuit equations that describe the DFIG machine, including the stator and rotor flux (current) dynamics and the rotor speed dynamics.

The 5th order model is derived in the synchronous coordinate system, also referred to as the d-q coordinate system. The q-axis of the rotating coordinate system is aligned with the grid voltage, and rotates at the nominal grid frequency of 50 Hz. The alignment with the grid voltage allows for simplifications of the circuit equations since the stator is connected directly to the grid. The q-component of the stator voltage will therefore appear to ”stand still” as it is aligned with the q-axis and rotating at the same speed. As a result, for a balanced 3-phase system and for balanced 3-phase-to-ground faults, $u_{sd} = 0$.

Figure 3.4 represents the equivalent electrical circuit of the dynamic DFIG model. This representation is referred to as the T-equivalent circuit, with the stator represented on the left, and the rotor on the right. The interface between the two is represented by the magnetizing inductance L_m, which also represents the air-gap in the machine and is commonly referred to as the air-gap flux. The stator terminals are connected directly to the grid through a step-up transformer, while the rotor is connected to the grid through back-to-back converters and an interconnection transformer. In this thesis the transformer ratios are assumed to be 1:1 for simplicity and are therefore not shown in the equivalent

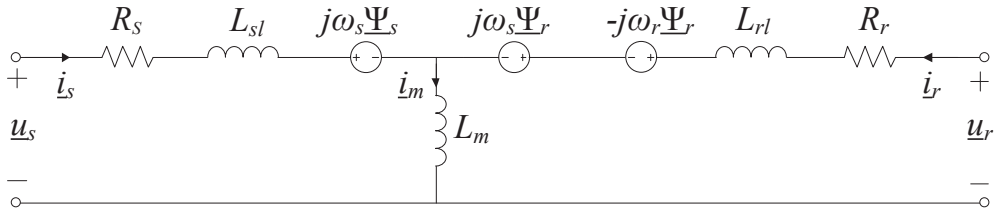

Figure 3.4: Equivalent electrical circuit of the DFIG

circuit. All calculations and derivations will be done in the motor reference frame, therefore positive power will represent power consumption while negative power will represent power production of both the stator and rotor.

The variables represented in Figure 3.4 are as follows:

$\underline{u}_s$ stator voltage (also grid voltage)
$\underline{u}_r$ rotor voltage
$\underline{\Psi}_s$ stator flux linkage
$\underline{\Psi}_r$ rotor flux linkage
$\underline{i}_s$ stator current
$\underline{i}_r$ rotor current
R_s stator resistance
R_r rotor resistance
L_s stator inductance
L_r rotor inductance
L_m magnetizing inductance
w_s grid frequency
w_r rotor frequency

3.2.1 Transient Model

The transient model developed here is used to define the behavior of the DFIG machine itself. This thesis uses space vector representation, with complex vectors represented as underlined variables. As mentioned previously, each complex vector will be represented by orthogonal direct (d) and quadrature (q) components, with the q-axis aligned with the

stator voltage.

Equations (3.1) through (3.4) below represent the mathematical relationships that define the behavior of the DFIG. All equations utilize nominal quantities unless per unit (p.u.) is specifically stated.

$$\underline{u}_s = R_s \underline{i}_s + \frac{d\underline{\Psi}_s}{dt} + j\omega_s \underline{\Psi}_s \tag{3.1}$$

$$\underline{u}_r = R_r \underline{i}_r + \frac{d\underline{\Psi}_r}{dt} + j(\omega_s - \omega_r)\underline{\Psi}_r \tag{3.2}$$

$$\underline{\Psi}_s = L_s \underline{i}_s + L_m \underline{i}_r \tag{3.3}$$

$$\underline{\Psi}_r = L_m \underline{i}_s + L_r \underline{i}_r \tag{3.4}$$

Equations (3.3) and (3.4) can be substituted into (3.1) and (3.2) to yield the following two equations, where the stator and rotor currents have been eliminated in order to simplify the equations in terms of stator and rotor flux only.

$$\underline{u}_s = (\frac{R_s}{L'_s} + j\omega_s)\underline{\Psi}_s + \frac{d\underline{\Psi}_s}{dt} - k_r \frac{R_s}{L'_s}\underline{\Psi}_r \tag{3.5}$$

$$\underline{u}_r = -k_s \frac{R_r}{L'_r}\underline{\Psi}_s + (\frac{R_r}{L'_r} + j(\omega_s - \omega_r))\underline{\Psi}_r + \frac{d\underline{\Psi}_r}{dt} \tag{3.6}$$

$$\tag{3.7}$$

where

$$\begin{aligned} k_s &= \frac{L_m}{L_s}, \\ k_r &= \frac{L_m}{L_r}, \\ L'_s &= \sigma L_s, \\ L'_r &= \sigma L_r, \\ \sigma &= 1 - k_s k_r \end{aligned}$$

Equations (3.5) and (3.6) are now set up in terms of stator and rotor flux linkages, and contain only a single derivative term. This allows the equations to be solved using the stator and rotor flux linkages as state variables in a state-space form.

In order to complete the characterization of the DFIG machine, the relationship between the electrodynamic torque, rotor speed, and flux linkages must be defined. First, the electrodynamic torque T_e can be defined as:

$$T_e = \frac{3}{2}p\frac{k_r}{L'_s}\Im[\underline{\Psi}^*_r\underline{\Psi}_s] = \frac{3}{2}p\frac{k_r}{L'_s}(\Psi_{rd}\Psi_{sq} - \Psi_{rq}\Psi_{sd}) \tag{3.8}$$

where $\Im$ is the imaginary part, and p represents the number of machine poles. The relationship between the electromagnetic torque produced by the machine, the load torque from the wind turbine T_L, and the rotor speed is defined in what is called the "swing" equation.

$$\frac{J}{p}\frac{d\omega_r}{dt} = T_e - T_L - b\frac{\omega_r}{p} \tag{3.9}$$

where J is the combined inertia of the machine and turbine in kgm^2 and b is the speed dependent damping term. This equation demonstrates that any imbalance in the electromagnetic torque T_e and load torque T_L will result in a change in the rotor speed, either acceleration or deceleration, represented as $\frac{d\omega_r}{dt}$. If T_e and T_L are equal, as in steady state, the rotor speed will reach its steady state value and the derivative term will therefore be zero. The swing equation is fundamental in describing and understanding the behavior of the DFIG during transient stability studies.

In order to use the swing equation in the state-space form, the equations (3.8) and (3.9) must be combined and described in terms of the state variables, which in this case are the flux linkages and rotor speed. The resulting equation is:

$$\frac{J}{p}\frac{d\omega_r}{dt} = \frac{3}{2}p\frac{k_r}{L'_s}(\Psi_{rd}\Psi_{sq} - \Psi_{rq}\Psi_{sd}) - T_L - b\frac{\omega_r}{p} \tag{3.10}$$

Simulink is used to solve the set of differential equations using the S-function feature. The equations for a state-space formulation are of the form:

$$\dot{\mathbf{x}} = A\mathbf{x} + B\mathbf{u}$$
$$\mathbf{y} = C\mathbf{x} + D\mathbf{u}$$

where **x** is the state variable vector, **y** is the output vector, **u** is the input vector, and vectors A through D are vectors defined by the system parameters.

Therefore, with the selected state variables of rotor flux, stator flux, and rotor speed, the derivatives of each ($\dot{\mathbf{x}}$) are solved for in (3.5), (3.6), and (3.10) to set up the following state-space representation of the differential equations:

$$\begin{bmatrix} \frac{d\Psi_{sd}}{dt} \\ \frac{d\Psi_{sq}}{dt} \\ \frac{d\Psi_{rd}}{dt} \\ \frac{d\Psi_{rq}}{dt} \\ \frac{d\omega_r}{dt} \end{bmatrix} = \begin{bmatrix} -\frac{R_s}{L'_s} & \omega_s & k_r\frac{R_s}{L'_s} & 0 & 0 \\ -\omega_s & -\frac{R_s}{L'_s} & 0 & k_r\frac{R_s}{L'_s} & 0 \\ k_s\frac{R_r}{L'_r} & 0 & -\frac{R_r}{L'_r} & \omega_s - \omega_r & 0 \\ 0 & k_s\frac{R_r}{L'_r} & \omega_r - \omega_s & -\frac{R_r}{L'_r} & 0 \\ 0 & \frac{3}{2}\frac{p^2}{J}\frac{k_r}{L'_s}\Psi_{rd} & 0 & -\frac{3}{2}\frac{p^2}{J}\frac{k_r}{L'_s}\Psi_{sd} & -\frac{b}{J} \end{bmatrix} \begin{bmatrix} \Psi_{sd} \\ \Psi_{sq} \\ \Psi_{rd} \\ \Psi_{rq} \\ \omega_r \end{bmatrix} +$$

$$\begin{bmatrix} 1 & 0 & 0 & 0 & 0 \\ 0 & 1 & 0 & 0 & 0 \\ 0 & 0 & 1 & 0 & 0 \\ 0 & 0 & 0 & 1 & 0 \\ 0 & 0 & 0 & 0 & -\frac{p}{J} \end{bmatrix} \begin{bmatrix} u_{sd} \\ u_{sq} \\ u_{rd} \\ u_{rq} \\ T_L \end{bmatrix} \tag{3.11}$$

With the rotor and stator flux linkages, the rotor and stator currents can be obtained from equations (3.3) and (3.4) as follows:

$$\underline{i}_s = \frac{\underline{\Psi}_s - k_r \underline{\Psi}_r}{L'_s} \tag{3.12}$$

$$\underline{i}_r = \frac{\underline{\Psi}_r - k_s \underline{\Psi}_s}{L'_r} \tag{3.13}$$

3.2.2 Γ-equivalent Model

The previous set of equations were derived in order to describe the DFIG machine itself. However, in order to derive the controller for the machine, the T-model of the equivalent circuit must first be transformed. The T-model contains a unique set of current and flux linkages for the stator and rotor side. In order to simplify and consolidate these variables, the stator leakage inductance can be moved to the rotor side, allowing the stator and rotor leakage inductance to be combined. This also allows the stator flux to be expressed in terms of the magnetizing inductance and magnetizing current. The resulting circuit is denoted the Γ-equivalent model. First, the transformation variable b is defined as

$$b = \frac{L_s}{L_m}$$

The transformation variable allows the parameters to be transformed from the T-equivalent model to the Γ-equivalent model. The following parameters are defined for the Γ-equivalent model, where an uppercase subscript is used to differentiate between the two models.

$$\begin{aligned} L_M &= bL_m = L_s \\ R_R &= b^2 R_r \\ L_\sigma &= bL_{sl} + b^2 L_{rl} = b^2 L_r - L_s \end{aligned}$$

The transformation variable b also allows for the following rotor side equivalent variables for the Γ-model:

$$\underline{i}_R = \frac{\underline{i}_r}{b} \tag{3.14}$$
$$\underline{\Psi}_R = b\underline{\Psi}_r \tag{3.15}$$
$$\underline{u}_R = b\underline{u}_r \tag{3.16}$$

The stator side variables can be transformed starting from the T-model equations. First, the stator flux can be expressed as:

$$\begin{aligned}\underline{\Psi}_s &= L_m\underline{i}_r + L_s\underline{i}_s \\ &= L_s(\frac{L_m}{L_s}\underline{i}_r + \underline{i}_s) \\ &= L_s(\frac{1}{b}\underline{i}_r + \underline{i}_s) \\ &= L_M(\underline{i}_R + \underline{i}_s)\end{aligned} \tag{3.17}$$

The stator voltage can be expressed as:

$$\begin{aligned}\underline{u}_s &= R_s\underline{i}_s + \frac{d\underline{\Psi}_s}{dt} + j\omega_s\underline{\Psi}_s \\ &= R_s\underline{i}_s + \frac{d(L_M(\underline{i}_r + \underline{i}_s))}{dt} + j\omega_s\underline{\Psi}_s \\ &= R_s\underline{i}_s + L_M\frac{d\underline{i}_M}{dt} + j\omega_s\underline{\Psi}_s\end{aligned} \tag{3.18}$$

The rotor flux for the Γ-model can be expressed as:

$$\begin{aligned}\underline{\Psi}_R &= b\underline{\Psi}_r \\ &= b(L_r\underline{i}_r + L_m\underline{i}_s) \\ &= b(b\underline{i}_R L_r + L_m\underline{i}_s) \\ &= b^2 L_r\underline{i}_R + L_M\underline{i}_s \\ &= \frac{L_\sigma + L_s}{L_r}L_r\underline{i}_R + L_M\underline{i}_s \\ &= L_\sigma\underline{i}_R + L_s\underline{i}_R + L_M\underline{i}_s \\ &= L_\sigma\underline{i}_R + \underline{\Psi}_s\end{aligned} \tag{3.19}$$

Finally the rotor voltage for the Γ-model can be expressed by multiplying b to the rotor voltage equation in (3.2):

$$\begin{aligned}
\underline{u}_R &= b\underline{u}_r \\
&= b(R_r\underline{i}_r) + b(\frac{d\underline{\Psi}_r}{dt}) + b(j(\omega_s - \omega_r)\underline{\Psi}_r) \\
&= R_R\underline{i}_R + \frac{d\underline{\Psi}_R}{dt} + j(\omega_s - \omega_r)\underline{\Psi}_R \\
&= R_R\underline{i}_R + L_\sigma\frac{d\underline{i}_R}{dt} + L_M\frac{d\underline{i}_M}{dt} + j(\omega_s - \omega_r)\underline{\Psi}_R \qquad (3.20)
\end{aligned}$$

Equations (3.18) and (3.20) can be used to set up the Γ-equivalent model as shown in Figure 3.5. These Γ-model equations will be used moving forward with the design of the various controllers.

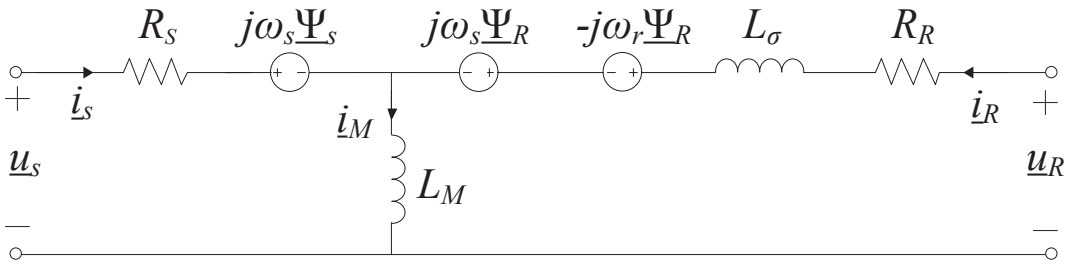

Figure 3.5: Γ-Equivalent electrical circuit of the DFIG, showing stator and rotor leakage inductance combined and allowing stator flux to be expressed in terms of magnetizing inductance and current.

3.3 Control of DFIG Machine

3.3.1 Rotor Current Controller

The rotor current controller controls the rotor current by calculating the required rotor voltage needed for a given reference current value. Therefore, the current controller must first define a system model of the DFIG machine, which can be done by deriving a transfer function from u_R to i_R. This can be accomplished by solving for $\frac{u_R}{i_R}$ from the previously derived equations describing the machine. First, the rotor voltage equation is transformed to eliminate i_M by solving equation (3.18) for $L_M\frac{di_M}{dt}$ and inserting into equation (3.20) as follows:

$$\underline{u}_R = R_R\underline{i}_R + L_\sigma\frac{d\underline{i}_R}{dt} + (\underline{u}_s - R_s\underline{i}_s - j\omega_s\underline{\Psi}_s) + j(\omega_s - \omega_r)\underline{\Psi}_R$$

Next, both the stator current $\underline{i}_s$ and rotor flux $\underline{\Psi}_R$ are eliminated:

$$\begin{aligned}\underline{u}_R &= R_R\underline{i}_R + L_\sigma\frac{d\underline{i}_R}{dt} + \underline{u}_s - R_s(\frac{\underline{\Psi}_s}{L_M} - \underline{i}_R) - j\omega_s\underline{\Psi}_s + j(\omega_s-\omega_r)(L_\sigma\underline{i}_R + \underline{\Psi}_s) \\ &= \underline{u}_s + L_\sigma\frac{d\underline{i}_R}{dt} + (R_s+R_R)\underline{i}_R + j(\omega_s-\omega_r)L_\sigma\underline{i}_R - \frac{R_s}{L_M}\underline{\Psi}_s - j\omega_r\underline{\Psi}_s \qquad (3.21)\end{aligned}$$

By taking the Laplace transform of equation (3.21), the rotor voltage equation results in the following:

$$\underline{u}_R = \underline{u}_s + \underline{i}_R(R_s + R_R + sL_\sigma) + j(\omega_s-\omega_r)L_\sigma\underline{i}_R - \frac{R_s}{L_M}\underline{\Psi}_s - j\omega_r\underline{\Psi}_s \qquad (3.22)$$

where the term $(\frac{R_s}{L_M} + j\omega_r)\underline{\Psi}_s$ is defined as the back EMF of the machine (**E**). As mentioned, it is desired to solve for the transfer function from u_R to i_R, which can be done by solving for $\frac{u_R}{i_R}$. As this cannot be done directly, the stator voltage $\underline{u}_s$ and machine back EMF **E** can be treated as disturbances, resulting in the following transfer function:

$$G_C = \frac{\underline{i}_R}{(\underline{u}_R - \underline{u}_s + \mathbf{E})} = \frac{1}{sL_\sigma + R_s + R_R + j(\omega_s-\omega_r)L_\sigma} \qquad (3.23)$$

For the derivation of the controller, the term $j(\omega_s-\omega_r)L_\sigma$ can be treated with a feed forward loop. The transfer function G_C is therefore reduced to simply:

$$G_C = \frac{1}{(sL_\sigma + R_s + R_R)} \qquad (3.24)$$

There are several methods in which a controller can be designed. The method that will used in this thesis is internal model control (IMC). IMC simply uses the knowledge of the system model to develop the control parameters required to augment the error between the actual system and the model of the system. The controller can be derived from the following relationship, where $F(s)$ represents the controller transfer function, and knowing that the control loop should behave like a first-order transfer function.

$$\begin{aligned}\frac{F(s)G(s)}{1+F(s)G(s)} &= \frac{\alpha}{s+\alpha} \\ F(s)G(s) &= \frac{\alpha}{s} \\ F(s) &= \frac{\alpha}{s}(sL_\sigma + R_s + R_R) \qquad (3.25)\end{aligned}$$

For a PI controller, $F(s)$ can be set equal to $k_p + \frac{k_i}{s}$, and the PI controller parameters derived as follows:

$$\begin{aligned} F(s) &= \frac{\alpha}{s}(sL_\sigma + R_s + R_R) = k_{pc} + \frac{k_{ic}}{s} \\ &= \alpha L_\sigma + \alpha\frac{(R_s + R_R)}{s} = k_{pc} + \frac{k_{ic}}{s} \end{aligned} \tag{3.26}$$

and therefore

$$k_{pc} = \alpha L_\sigma \tag{3.27}$$

$$k_{ic} = \alpha(R_s + R_R) \tag{3.28}$$

With these control parameters, and using equation (3.22), the reference values for the rotor voltage can be obtained from the following equations:

$$\begin{aligned} u_{Rd}^{ref} = (k_{pc} + \frac{k_{ic}}{s})(i_{Rd}^{ref} - i_{Rd}) + u_{sd} &- (\omega_s - \omega_r)L_\sigma i_{Rq} \\ &- \frac{R_s}{L_M}\Psi_{sd} + \omega_r\Psi_{sq} \end{aligned} \tag{3.29}$$

$$\begin{aligned} u_{Rq}^{ref} = (k_{pc} + \frac{k_{ic}}{s})(i_{Rq}^{ref} - i_{Rq}) + u_{sq} &+ (\omega_s - \omega_r)L_\sigma i_{Rd} \\ &- \frac{R_s}{L_M}\Psi_{sq} - \omega_r\Psi_{sd} \end{aligned} \tag{3.30}$$

3.3.2 Active Damping R_a

An additional term can be included in the design of the current controller, called ”active resistance”, or R_a. The active resistance is added to the actual machine resistance values in the transfer function, and gives additional flexibility in damping out variations of the back emf. This resistance is not ”real” in the sense that it is not physically present in the machine, but is added purely for a higher level of control. When introducing an active resistance, the controller gains must be updated to account for R_a. The new controller gains are

$$k_{pc} = \alpha L_\sigma \tag{3.31}$$

$$k_{ic} = \alpha(R_s + R_R + R_a) \tag{3.32}$$

3.3.3 Rotor Current Reference Calculation

The reference values for the rotor current can be derived directly from the equations that describe the electrodynamic torque of the machine and the stator reactive power.

q-axis rotor current reference calculation

First, the equation for the electrodynamic torque is revised to include the rotor current. It is important to note that there are several ways in which the electrodynamic torque can be expressed, and throughout the literature on this topic a variety of forms of the equation are presented. It can be shown algebraically that these equations are all equivalent. The following is the equation used for the purposes of deriving the rotor current reference values.

$$\begin{aligned} T_e &= -\frac{3}{2}p\Im[\underline{\Psi}_s^* \underline{i}_R] \\ &= -\frac{3}{2}p\Im[(\Psi_{sd} - j\Psi_{sq})(i_{Rd} + ji_{Rq}] \\ &= -\frac{3}{2}p(\Psi_{sd} i_{Rq} - \Psi_{sq} i_{Rd}) \end{aligned} \tag{3.33}$$

As was discussed previously, the d-q coordinate system for this thesis has aligned the stator voltage with the q-axis. Therefore, $u_{sd} = 0$. Equation (3.18), which describes the stator voltage for the Γ-model, can be used to simplify equation (3.33). With the assumptions that $R_s = 0$ (R_s is in fact a very small value), and that the machine operates in steady-state (which allows the derivative term to be set equal to 0), then $\Psi_{sq} = 0$. Since it is difficult to measure the torque, it is often commonly controlled with an open loop [5]. Equation (3.33) can then be simplified to yield the equation for the q-axis rotor current reference value.

$$\begin{aligned} T_e &= -\frac{3}{2}p(\Psi_{sd} i_{Rq}) \\ i_{Rq}^{ref} &= -\frac{2}{3p}\frac{T_e^{ref}}{\Psi_{sd}} \end{aligned} \tag{3.34}$$

The simplifications and assumptions used to derive i_{Rq}^{ref} do have an impact on the controllability of the torque. The i_{Rq}^{ref} that is fed into the current controller in order to achieve the reference torque value is not accurate because it does not take into account the stator resistance. Therefore, the actual torque of the machine will always differ from the reference torque, resulting in a steady-state error. If the mechanical torque T_m is set equal to

the reference torque T_e^{ref}, as is common to do, the steady state difference between the two will result in a continuous increase or decrease of the rotor speed due to the swing equation defined in equation (3.9). This can be corrected with a speed controller in cascade with the current controller that is used to adjust T_e^{ref} in order to keep the rotor speed constant. Another alternative is to use an active power controller to derive i_{Rq}^{ref}. These two options are elaborated in the following sections.

d-axis rotor current reference calculation

The d-axis rotor current reference value can be derived from an understanding of the stator reactive power. i_{Rd}^{ref} is derived as follows:

$$\begin{aligned} Q_s &= \frac{3}{2}\Im[\underline{u}_s\underline{i}_s^*] \\ &= \frac{3}{2}\Im[(R_s\underline{i}_s + L_M\frac{d\underline{i}_M}{dt} + j\omega_s\underline{\Psi}_s)(\frac{\underline{\Psi}_s}{L_M} - \underline{i}_R)^*] \end{aligned}$$

and assuming $R_s = 0$ and steady state conditions, simplifies to

$$\begin{aligned} Q_s &= \frac{3}{2}\Im[j\omega_s\underline{\Psi}_s)(\frac{\underline{\Psi}_s}{L_M} - \underline{i}_R)^*] \\ &= \frac{3}{2}u_{sq}(\frac{\Psi_{sd}}{L_M} - i_{Rd}) \end{aligned} \tag{3.35}$$

Equation (3.35) can be used directly to solve for the i_{Rd}^{ref} value.

$$i_{Rd}^{ref} = \frac{\Psi_{sd}}{L_M} - \frac{2}{3}\frac{Q_s^{ref}}{u_{sq}} \tag{3.36}$$

The equation (3.36) represents control of i_{Rd}^{ref} in an open loop manner. The following section expands on using Q_s to control i_{Rd} in a closed-loop control system.

3.3.4 Reactive Power (Q) Controller

For the DFIG machine in a wind turbine application, it is desirable to control the reactive power. In steady-state, the controller should keep the reactive power set equal to zero, therefore maximizing the active power injection to the grid. During a fault condition where the grid voltage drops, it may be desirable to inject reactive power from the DFIG in order to provide voltage support. The magnitude and duration of reactive power

injection is dependent on the requirements of the local grid codes, to be explained in more detail later in this thesis.

The DFIG has two connections to the grid, allowing for reactive power injection and consumption to be controlled through either the rotor or stator circuit. In practice, the GSC in the rotor circuit always controls the reactive power to zero. The RSC in the rotor circuit can be used to control the stator reactive power by controlling i_{Rd}^{ref}, and it is through the control of i_{Rd}^{ref} that the DFIG is able to provide reactive power support during grid voltage dips. Equation (3.35) can be used to derive the reactive power controller parameters.

First, the transfer function G_Q from Q_s to i_{Rd} can be defined as

$$G_Q = \frac{Q_s}{i_{Rd} - \frac{\Psi_{sd}}{L_M}} = -\frac{3}{2}u_{sq} \tag{3.37}$$

The controller $F_Q(s)$ can be defined using internal model control as was shown in equation (3.25) to yield the following relationship

$$F_Q(s) = \frac{\alpha_Q}{s}G_Q^{-1}(s) = -\frac{2\alpha_Q}{3u_{sq}}\frac{1}{s} \tag{3.38}$$

In deriving the controller it is shown that only an I-controller is needed using the internal model control method. The gain of the controller $k_{iQ} = -\frac{2\alpha_Q}{3u_{sq}}$. In this thesis, the Q controller is implemented with an I-controller only with a bandwidth initially set to 100 rad/s (10 times slower than the initial setting of the current controller bandwidth).

For this thesis, during steady state and normal operation, the reactive power output of the DFIG machine will be set to zero ($Q_{gc} = Q_s = 0$), and the machine will prioritize active power output. During voltage dips, all models will implement the E.ON grid code reactive power requirement as previously described. This requires reactive power to be supplied by the DFIG machine for all voltage dips less than 0.9 p.u., and is a function of the severity of the voltage dip. This acts to prioritize reactive power output during voltage dips, and only provide real power if there is sufficient capacity left without exceeding the rotor current limitations.

3.3.5 Speed Controller

A speed controller can be used in cascade with the current controller to control the rotor speed to a constant steady-state value. The rotor speed reference value can be obtained based on the power-speed relationship of the wind turbine, typically in the form of a table. This table shows the relationship of rotor speed on the input mechanical power (or mechanical torque). The actual rotor speed can thus be measured and compared to the

reference value, with the controller giving a torque reference that is fed into the current controller.

The rotor speed dynamics are reasonably slow when compared to the time of a voltage dip event. Voltage dips commonly last less than one second. This thesis analyzed the rotor speed dynamics during the voltage dip to determine if an assumption of a fixed rotor speed is valid for transient stability and voltage stability studies.

In this thesis, a speed controller was implemented in one of the detailed model iterations for the purposes of comparison and to analyze the impact to the results. The controller was derived using internal model control, using the swing equation of

$$\frac{J}{p}\frac{d\omega_r}{dt} = T_e - T_L - B\omega_r \tag{3.39}$$

where B is the speed dependent damping term. In this equation, T_e is set equal to T_e^{ref} and the load torque T_L is treated as a disturbance. Therefore, the transfer function $G_\omega(s)$ can be found by taking the Laplace transform and solving for the ratio of T_e^{ref} to ω_r, resulting in the following equation

$$G_\omega = \frac{T_e^{ref}}{\omega_r} = \frac{J}{p}s + B \tag{3.40}$$

yielding the following controller equation

$$F_\omega(s) = \frac{\alpha_\omega}{s}G_\omega^{-1}(s) = \alpha_\omega\frac{J}{p} + \alpha_\omega\frac{B}{s} \tag{3.41}$$

The controller parameters can be taken directly from (3.41) as $k_p = \alpha_\omega\frac{J}{p}$ and $k_i = \alpha_\omega B$. The speed controller bandwidth for this thesis was set to be slower than the inner loop control at $100\frac{rad}{s}$.

When using a speed controller, considerations must be taken regarding high versus low wind speeds. During low wind speeds, before the wind turbine has reached rated power output, each wind speed corresponds to a unique power value. However, when the wind speed increases and the wind turbine reaches rated power, the wind speed is used to control the pitch and not the power. This results in two controllers that are dependent on the wind speed - one controller that gives a torque or power reference (low wind speeds), and one controller that gives a pitch reference (high wind speeds). The controller must switch between the two modes dependent on the wind speed.

3.3.6 Active Power (P) Controller

An active power controller can also be used in cascade with the current controller in lieu of the speed controller. In this case, the reference power value is obtained from the wind turbine's power-speed relationship, representing the mechanical power into the machine. This value is compared to the actual active power output, which is calculated from the sum of the stator power (P_s) and the grid-side converter power (P_{GC}).

For the purposes of this thesis, a simulation is performed for one operating point at a time. For example, the wind turbines may be modeled at rated power for a given voltage dip to study the effects of voltage and transient stability on the system. The simulation does not dynamically change between operating points. For this reason, when operating at just one operating point, an active power controller may be considered equivalent to a speed controller. The advantage of using an active power controller is that it is not necessary to switch between control modes for high and low wind speeds. The model can be used for the full range of operation. For this reason, a P controller is used for outer loop control in lieu of a speed controller.

The power controller was derived using internal model control using the torque relationship of (3.33) and the relationship between power and torque as follows

$$i_{Rq}^{ref} = -\frac{2}{3p}\frac{T_e^{ref}}{\Psi_{sd}} \tag{3.42}$$

and

$$P = T\Omega \tag{3.43}$$

yield the transfer function $G_P(s)$ of

$$G_P = \frac{P_{ref}}{i_{Rq}} = -\frac{3}{2}p\Psi_{sd}\Omega \tag{3.44}$$

yielding the following controller $F_P(s)$

$$F_P(s) = \frac{\alpha_p}{s}G_p^{-1}(s) = -\frac{\alpha_p}{s}\frac{2}{3p\Psi_{sd}\Omega} \tag{3.45}$$

This results in an integrator only controller. By substituting $\Omega = \frac{\omega_r}{p}$, and realizing the steady state relationship of $\Psi_{sd} = \frac{u_{sq}}{\omega_s}$, the integrator parameter k_i can be found as $-\frac{2\omega_s}{3u_{sq}\omega_r}$.

Chapter 4

Converter limitations and model implementation of DC-chopper

The rotor-side converter and grid-side converter have physical limitations that must be accounted for in the model. It is typical to have the converters in a DFIG wind turbine system sized at around 30% of the rated power of the generator. The limitation is realized in the form of both voltage and current limitations. A full model of these limitations would require implementation of a DC-link controller to properly model the DC-link voltage during transients. The control of DC-link voltage impacts the action of the DC crowbar used to release energy and protect the DC-link from overvoltage. As the intent of this thesis is to develop a simplified model for implementation in PSS/E, the DC-chopper controller is considered to act instantaneously with respect to the time step of the PSS/E simulation and is therefore not implemented in this thesis.

This section will describe how the voltage and current limitations on the rotor circuit are modeled in this thesis. It will also describe the operation of the DC-chopper, and how the DC-chopper was implemented in the detailed model.

4.1 Rotor voltage limitation

The RSC controls the rotor voltage $\underline{u}_R$ to obtain the desired current $\underline{i}_R$ required to control the torque and reactive power of the machine. If under certain conditions, the rotor voltage required to meet these demands is increased beyond a certain threshold, the converter will clamp the voltage and limit it to this amount. In this thesis, the maximum rotor voltage was determined based on the analysis of the 2MW wind turbine done in the Tvåker report [8]. The result of clamping the voltage causes higher rotor currents. This is illustrated in figures 4.1 through 4.4 below. The basic 5th order machine model with P and Q controllers

is compared to the same model but with a rotor voltage limitation. The actual limit of the rotor voltage is determined by the relationship with the DC-link voltage. This relationship will be described in more detail in the subsequent section.

Due to the poorly damped poles, the oscillations experienced during voltage dips are very high. The rotor currents exceed the maximum current by a large amount and cause the RSC to operate at maximum voltage for an extended period of time. This affects the ability of the RSC to control the P and Q output.

4.2 Rotor current limitation

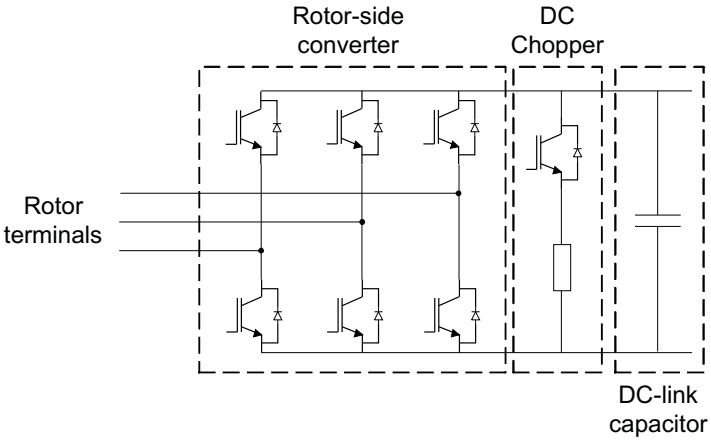

Figure 4.5: Rotor-side converter with DC-link

In a fully detailed model with a DC-link controller, the activation of the DC-chopper can be modeled by first monitoring the DC-link voltage. Refer to figure 4.5 for a representation of the RSC with DC-link. During a grid fault, there is a quick drop in the stator voltage. This causes an increase in the stator current (because of the controller's attempt to maintain the reference power output), which causes an increase in the rotor current. If the new $\underline{i}_r$ can be achieved, then the power output remains unchanged. However if the new $\underline{i}_r$ cannot be achieved, then P_s will decrease and P_r will increase.

When higher rotor currents are required, the RSC attempts to increase the rotor voltage applied to the rotor circuit. This will work until the applied voltage reaches the maximum limit, which forces the RSC to clamp the voltage. However, by clamping the rotor voltage, the rotor circuit will experience an increase in the rotor current. Eventually a high rotor current will exceed the limit of the IGBT's in the RSC, and the RSC will subsequently send a turn-off signal to the IGBT's resulting in current flow through the freewheeling diodes. When this occurs, the RSC has lost controllability of the rotor circuit voltage, and

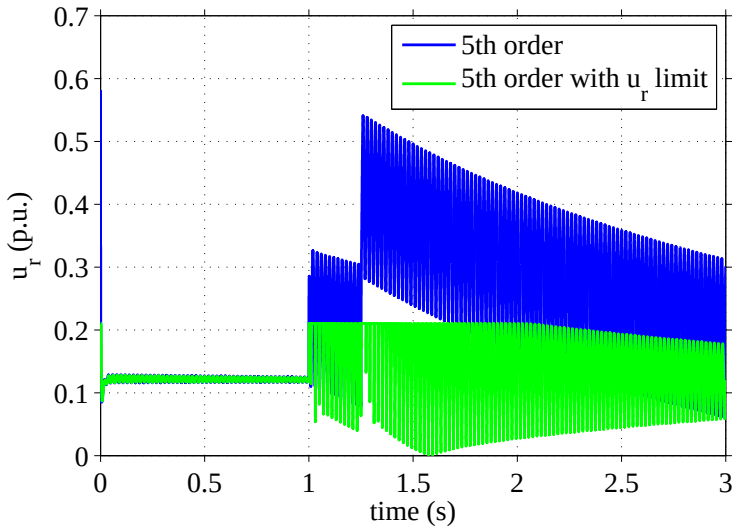

(a) u_r with and without rotor voltage limitation

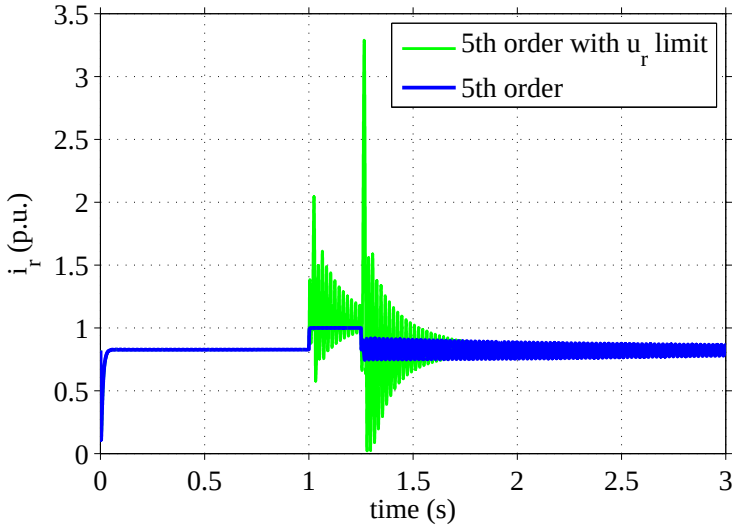

(b) i_r with and without rotor voltage limitation

Figure 4.1: u_r and i_r, super synchronous operation, 0.8 p.u. voltage dip, with and without rotor voltage limitation. The figures demonstrate how the clamping of the rotor voltage results in an increase in the rotor currents

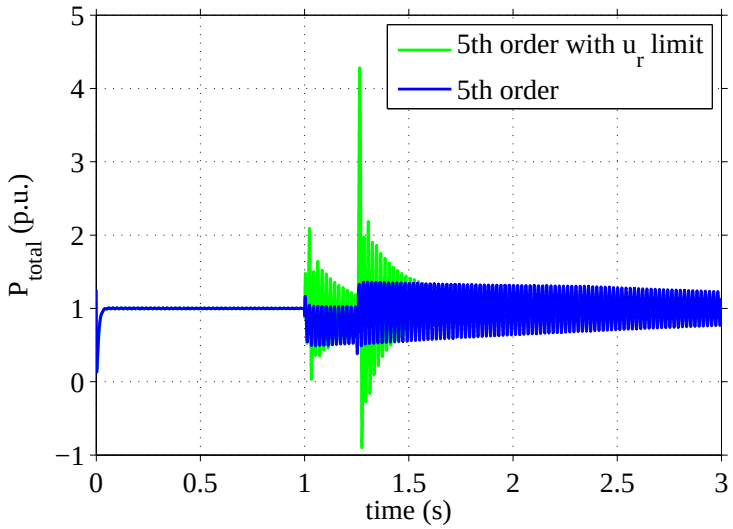

(a) P_{total} with and without rotor voltage limitation

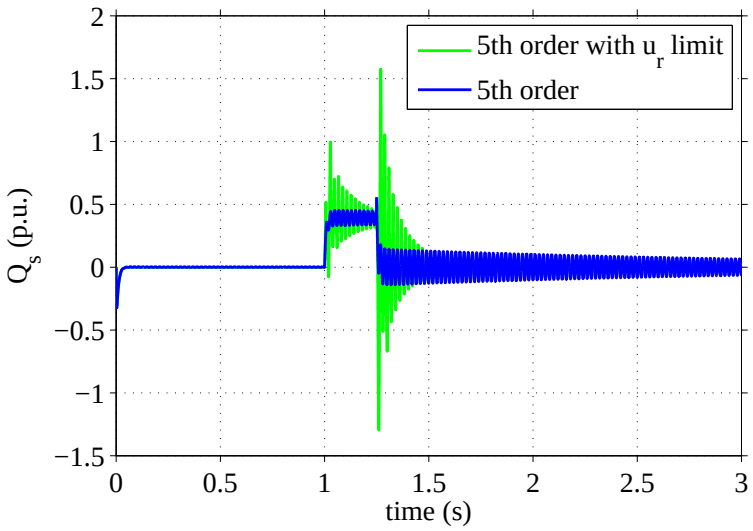

(b) Q_s with and without rotor voltage limitation

Figure 4.2: P_{total} and Q_s, super synchronous operation, 0.8 p.u. voltage dip, with and without rotor voltage limitation. The figures demonstrate how the clamping of the rotor voltage results in high transients on the power output.

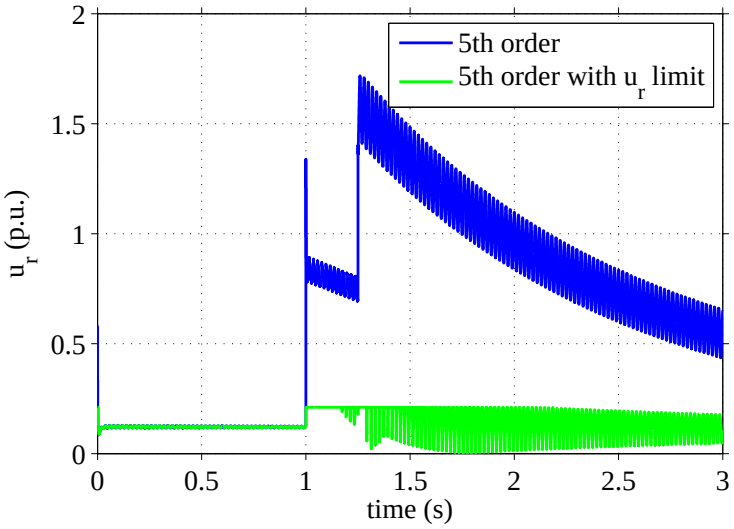

(a) u_r with and without rotor voltage limitation

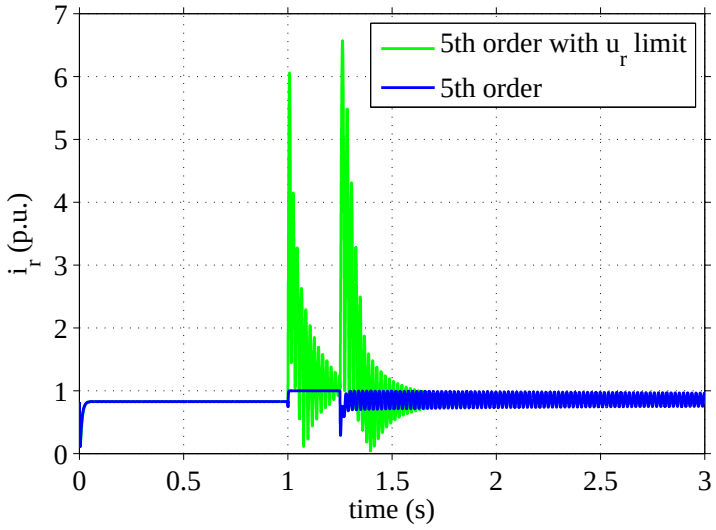

(b) i_r with and without rotor voltage limitation

Figure 4.3: u_r and i_r, super synchronous operation, 0.25 p.u. voltage dip, with and without rotor voltage limitation. The figures demonstrate how the clamping of the rotor voltage results in an increase in the rotor currents

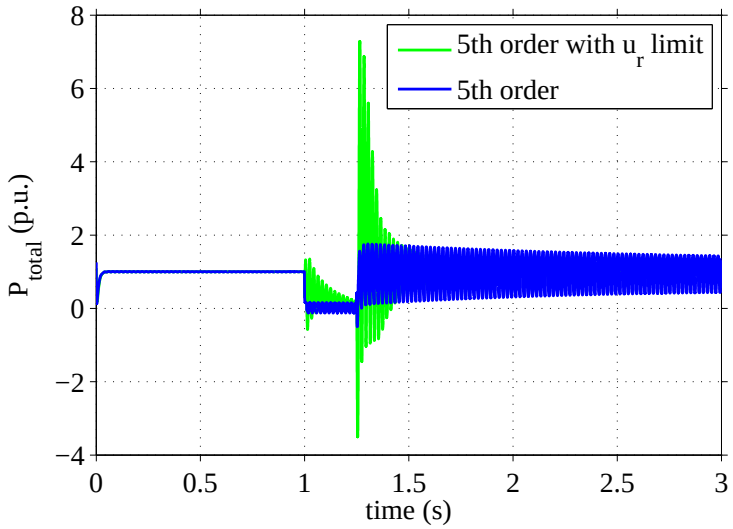

(a) P_{total} with and without rotor voltage limitation

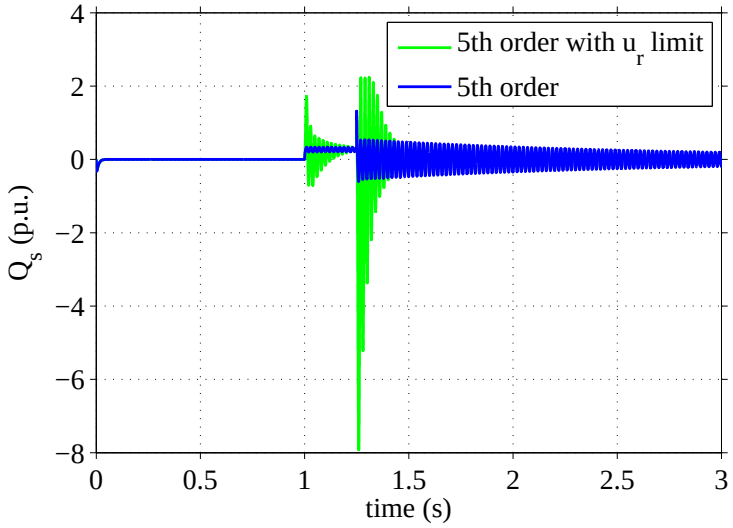

(b) Q_s with and without rotor voltage limitation

Figure 4.4: P_{total} and Q_s, super synchronous operation, 0.25 p.u. voltage dip, with and without rotor voltage limitation. The figures demonstrate how the clamping of the rotor voltage results in high transients on the power output.

has become a diode rectifier. The rotor current will begin to charge the DC-link capacitor and cause an increase to the DC-link voltage. When $U_{dc} > 1.12p.u.$, the DC-chopper is activated to release energy through the DC-chopper resistor. Refer to figure 4.6.

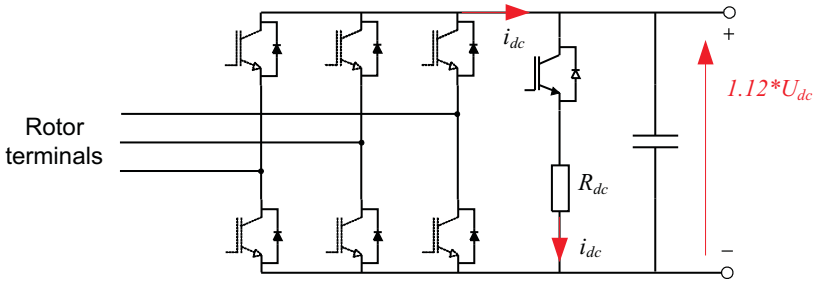

Figure 4.6: Rotor-side converter with DC-link

The DFIG can still be described by the same equations as before, however the rotor voltage magnitude is now determined by the DC-link voltage alone. The phase angle of the rotor voltage is equal to the phase angle of the rotor current, since the crowbar is a pure resistor (power factor = 1.0). The rotor voltage magnitude can be described with the following equation representing the relationship between phase voltage and DC-link voltage of a diode rectifier [9].

$$u_{R,phase} = \frac{U_{dc}\pi}{3\sqrt{3}} \tag{4.1}$$

The equation used to derive the rotor voltage during diode rectification is based on a diode rectifier with a current stiff DC source. For the case of the RSC and DC-link used in this thesis, it is more appropriate to consider the system with a constant DC-side voltage. However it is shown in [9] that this voltage relationship can still be used as an approximation.

4.3 Grid-side converter current limitation

Similar to the RSC, the GSC is limited based on the rating of the converter components. As discussed previously, the rotor circuit is designed to withstand around 30% of the rated generator power. This value is determined by the allowable range of the rotor speed around synchronous speed, as this determines the slip power and thus the power flowing through the rotor circuit.

The grid side converter active power can be calculated with:

$$P_{gc} = 1.5(u_{gcd}i_{gcd} + u_{gcq}i_{gcq}) \tag{4.2}$$

The voltage $\underline{u}_{gc}$ is set equal to the grid voltage, therefore:

$$\begin{aligned} u_{gcd} &= u_{sd} = 0 \\ u_{gcq} &= u_{sq} \end{aligned}$$

yielding the final equation for P_{gc} as:

$$P_{gc} = 1.5 N_{gs} u_{sq} i_{gcq}) \tag{4.3}$$

where N_{gs} represents the turns ratio of the transformer between the GSC and the stator. In this thesis, all transformers are modeled with a turns ratio equal to 1.

Similarly, the grid side converter reactive power can be calculated as:

$$\begin{aligned} Q_{gc} &= 1.5(u_{gcq} i_{gcd} - u_{gcd} i_{gcq}) \\ &= 1.5(u_{gcq} i_{gcd}) \\ &= 1.5 N_{gs} u_{sq} i_{gcd} \end{aligned} \tag{4.4}$$

This allows for the equations describing the dq grid side converter currents as:

$$i_{gcd} = \frac{Q_{gc}}{1.5 N_{gs} u_{sq}} \tag{4.5}$$

$$i_{gcq} = \frac{P_{gc}}{1.5 N_{gs} u_{sq}} \tag{4.6}$$

The total GSC current $|i_{gc}|$ is limited by the GSC to a certain value, $i_{gc,max}$. In this thesis, the sizing of the VSCs is based on their ability to handle 30% of the rated generator power. Therefore, the maximum GSC current is set to 0.3 p.u.

The active power that flows through the RSC must also flow through the GSC before reaching the grid. Therefore in the calculation of the GSC current, P_{gc} can be set equal to P_r, as long as the resulting GSC current does not exceed the maximum value. The reactive power is typically controlled to be zero, therefore $Q_{gc} = 0$.

4.4 Model implementation of DC-chopper

The main goal of implementing the DC-chopper in the 5th order detailed model is to understand the effects of the DC-chopper action on the overall energy balance and energy

transfer of the machine and the grid. Since the end goal of this model is to simplify it for use as a positive sequence model for modeling active and reactive power during grid faults, it is not necessary to simulate the actual power consumed by the DC-chopper or the variations in the DC-link voltage during the chopper action, as long as the interchange of power with the grid is properly represented.

The approach taken to calculate $\underline{u_r}$ during crowbar operation was to look at the steps taken by the RSC when moving from the controllable range to DC-chopper operation.

- The VSC output reaches its maximum value ($u_{r,max}$)
- The RSC will lose control instantaneously when $|i_r| > i_{r,max}$
- When the RSC loses controllability, the rotor voltage magnitude will be locked to the maximum rotor voltage, as derived from equation (4.1) based on the nominal DC-link voltage
- When the RSC loses controllability, the rotor voltage phase angle will be set equal to the rotor current phase angle
- The loss of RSC control signifies the switch to a diode rectifier, and thus the change in rotor voltage. Any excess energy caused by a difference in the rotor active power and grid-side active power is assumed to be burned in the DC crowbar resistor.

Therefore, to analyze the effects of the DC-chopper operation, the model implements a switch that changes the rotor voltage based on the operation of a diode rectifier. The switch is activated when the rotor current exceeds its maximum value. The rotor voltage magnitude is fixed at the maximum value as determined by the DC-link voltage (equation (4.1)), and the rotor voltage angle is switched to be in phase with the rotor current. Based on the use of the motor convention in this thesis, where positive power is going into the machine, the rotor voltage must actually be 180 degrees out of phase with the rotor current to simulate active power going from the machine to the DC-link during diode rectifier operation. For the purposes of this discussion, this model will be described as though the RSC maintains control throughout since it incorporates the base current controller only (without consideration of what happens when the current limitation is reached). This assumption is not entirely true as the current controller cannot achieve the desired reference rotor voltage during saturation.

Figure 4.7 shows a comparison of the model with the diode rectifier implemented, and without the diode rectifier implemented (5th order model with rotor voltage limitation), when applying a voltage dip of 0.8 p.u.. It can be seen in this figure that the rotor current decreases more quickly during the fault when the diode rectifier is implemented. The figure also shows how the rotor voltage magnitude remains clamped during diode rectifier

operation. Figure 4.8 shows a comparison of P_{total} and Q with and without the diode rectifier implemented. In figure 4.9, a deep voltage dip of 0.25 p.u. was applied for super synchronous operation (full power operation), and the resulting effects of P and Q shown. As with the shallow voltage dip, the P and Q responses are similar between the two models.

In summary, the responses in P and Q for the model including the diode rectifier are in good agreement with the model without the diode rectifier. Therefore, moving forward with model simplifications, the DC-chopper implementation will not be included in the model.

4.4.1 Regaining control of the RSC

In the previously described representation of the DFIG, the RSC loses control and changes to a diode rectifier purely based on the magnitude of $\underline{i}_r$. The converter switches back and forth between being in control and losing control based on the inequality $|i_r| \leq i_{r,max}$. However, it is of interest to investigate an alternative method to regaining control of the RSC by studying the rotor voltage when the RSC has lost control and is in diode rectifier mode. To do this, the rotor voltage reference is calculated by the current controller and then applied to a separate machine model in parallel with the model implementing the diode rectifier. Recall that this calculated reference rotor voltage will not be the same as the rotor voltage in the diode rectifier model, as the diode rectifier model will force the reference rotor voltage to be in phase with the rotor current. The resulting rotor current from the parallel model is analyzed to determine if the reference rotor voltage would result in a rotor current that does not exceed the maximum limit. In other words, the idea is to investigate what the rotor voltage would be if the RSC were to regain control, based on the current states of the system, and see what the resulting rotor current would be if this new rotor voltage were applied. This analysis would show the possibility of switching back *out* of diode rectifier mode and regaining control of the machine more quickly.

Figure 4.10 represents the magnitude of the rotor current for two different scenarios. The first scenario is simply the present model with the diode rectifier implemented. Therefore the RSC loses control and switches to a diode rectifier when the rotor current exceeds its maximum value. The second scenario is a representation of what the rotor current would be if the RSC were to regain control and apply the corresponding rotor voltage. The area of interest is any location where the rotor current from the controlled scenario dips below the maximum rotor current value (in this figure the value is 1.0 p.u.). When the rotor current goes below 1.0 p.u., it is of interest to see if the RSC is in control or out of control at that time instant. If it is not in control, there is an opportunity to regain control more quickly than by waiting for the rotor current to drop below the maximum limit.

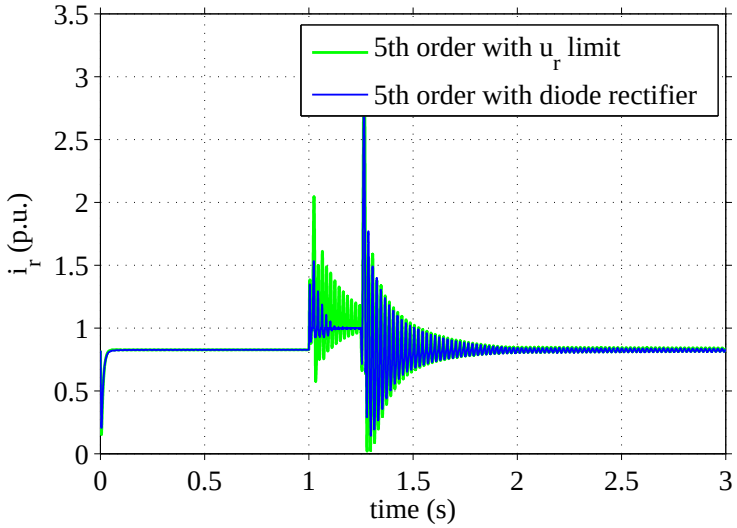

(a) i_r with and without diode rectifier implemented

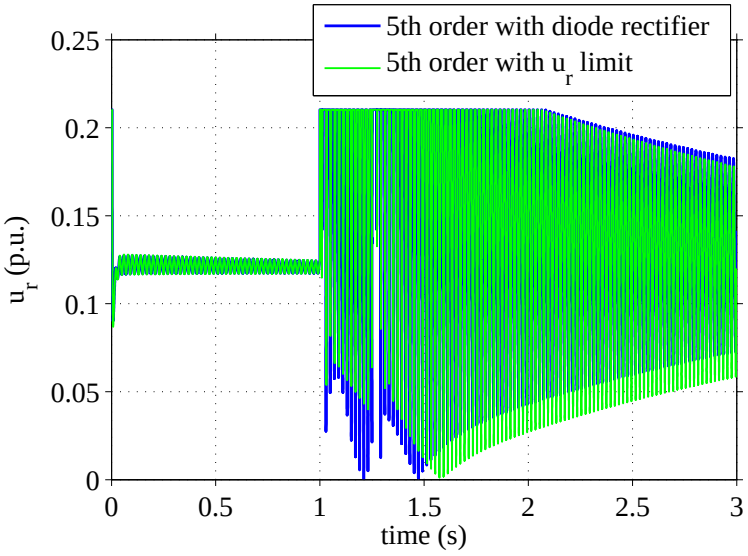

(b) u_r with and without diode rectifier implemented

Figure 4.7: i_r and u_r with and without diode rectifier implemented, for super synchronous operation, 0.8 p.u. voltage dip.

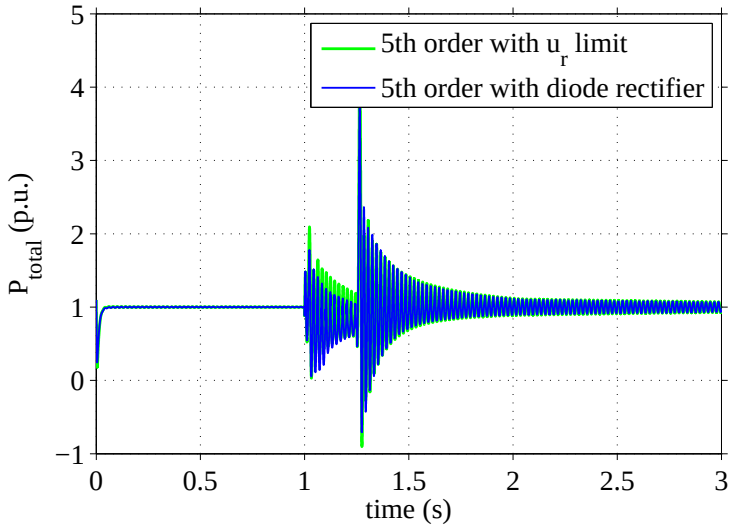

(a) P_{total} with and without diode rectifier implemented

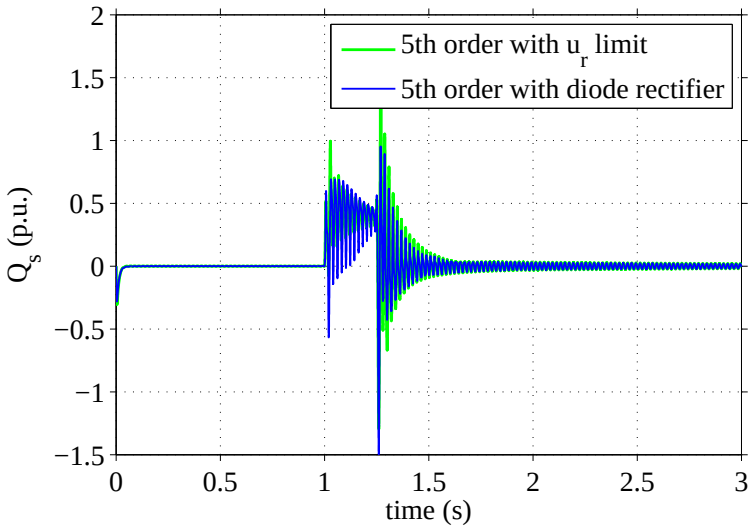

(b) Q_s with and without diode rectifier implemented

Figure 4.8: P_{total} and Q_s with and without diode rectifier implemented, for super synchronous operation, 0.8 p.u. voltage dip.

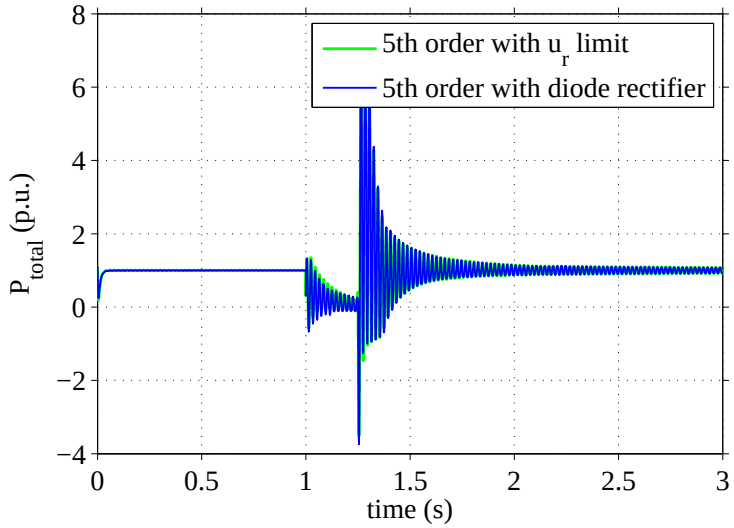

(a) P_{total} with and without diode rectifier implemented

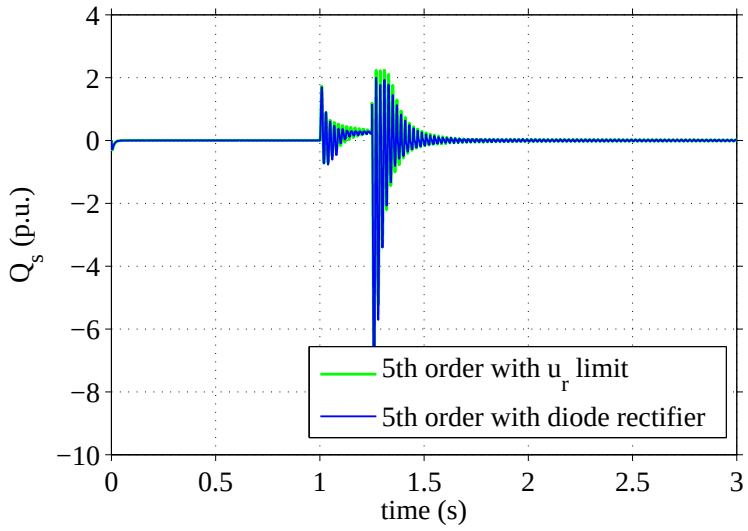

(b) Q_s with and without diode rectifier implemented

Figure 4.9: P_{total} and Q_s with and without diode rectifier implemented, for super synchronous operation, 0.25 p.u. voltage dip.

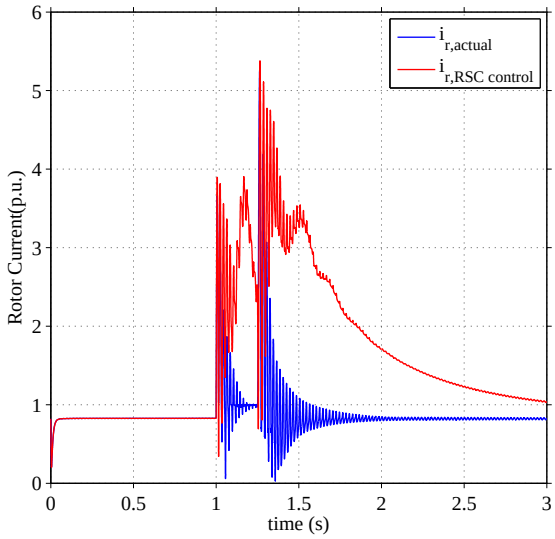

(a) The actual i_r with diode rectifier implemented, and i_r if the RSC was in control at all times.

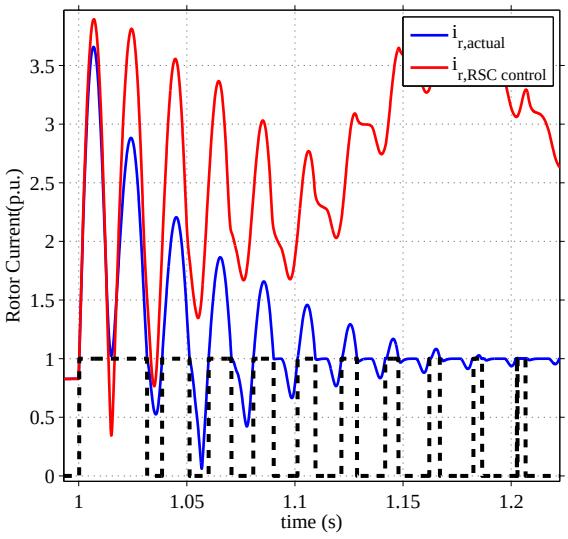

(b) Enlarged view.

Figure 4.10: The actual i_r and i_r that could be achieved if the RSC was in control. The switching between control mode and diode rectifier mode is represented by the black dashed line. As can be seen, the switching occurs when i_r decreases below 1.0 p.u.

Chapter 5

Evaluation of 5th Order Model against PSCAD Detailed Model

In an effort to validate the detailed model derived in this thesis, the model was compared against a more detailed model developed in PSCAD. This PSCAD model has been validated against the field measurements of an actual DFIG wind turbine subject to both an unbalanced shallow voltage dip and a more severe voltage dip where the voltage dropped to zero for a period of 70 ms. The PSCAD model showed excellent agreement with the field measurements [1].

The PSCAD model contains the following design features:

- Full converter PWM switching
- Grid side filter
- DC-link controller, for control of the DC link voltage
- Grid-side converter controller
- Both the P and Q controllers implemented as PI controllers
- Current controller implemented as a P controller only
- A slow rotor speed controller (10 rad/s) to ensure steady-state speed prior to voltage dip
- DC-chopper set to act on DC-link overvoltage

The detailed model was synchronized to the PSCAD model by the following actions:

- Synchronization of machine parameters

- Synchronization of controller parameters
- Field measured grid voltage applied as an input to 5th order model stator voltage

Figure 5.1 represents the field measured three-phase voltages during the severe voltage dip. During this event the voltage was depressed to almost zero for a period of 70 ms. The measured response of the wind turbine's active power is shown in figure 5.2(a). The operating point for this scenario was at around 0.52MW prior to the voltage dip. During the voltage dip, there is a Fault Ride Through (FRT) algorithm that controls the active power to 0 pu in order to make room for reactive power injection. After the fault is cleared, the controller waits for a dead-time period before ramping back up to the pre-fault value. This action is specific to the control algorithm of this specific wind turbine and is not considered a standard action, although most wind turbines do operate under certain FRT and reactive power requirements from the grid operator. The 5th order model was modified to simulate this FRT action by changing $P^{ref} = 0$ during the fault.

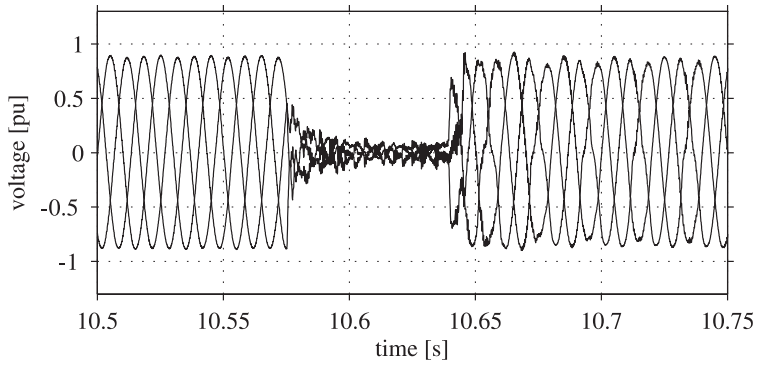

Figure 5.1: Field measurements for severe voltage dip experienced by DFIG wind turbine.

Figure 5.2(b) shows the 5th order model response of the active power. It can be seen from these figures that there are some general similarities to the response of the field measurements, but also some significant differences. First, the poor damping of the 5th order model is magnified in this simulation. Oscillations occur prior to the fault, in the prefault period, most likely caused by the small variations in the applied voltage. This leads to an assumption that any disturbances to the system cause the model to become less stable, with poorly damped oscillations of 50 Hz. The oscillations are exacerbated when the fault clears, with per-unit values much higher than the field measurements. The issue of poorly damped oscillations is studied in the following section. Second, the overall shape of the response is slightly different. The field measured data shows a large negative oscillation after the fault occurs that does not appear in the 5th order model. In addition, when the fault clears, the field measurements show a large positive oscillation that does not appear in the 5th order model.

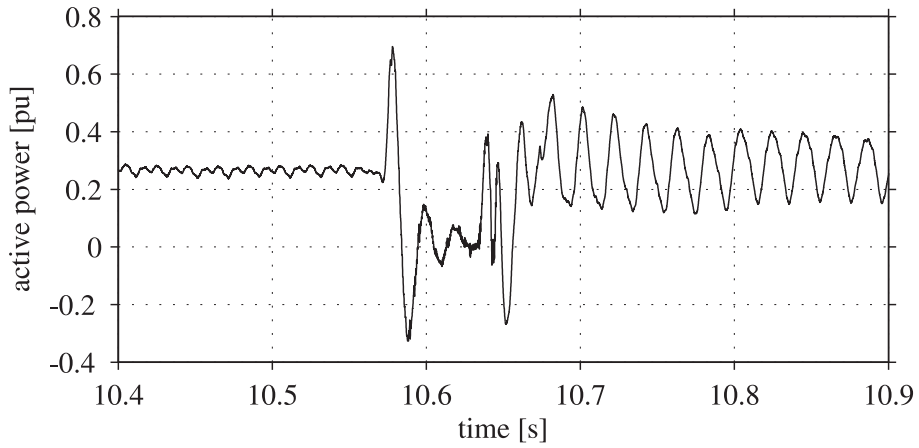

(a) Measured active power during severe voltage dip.

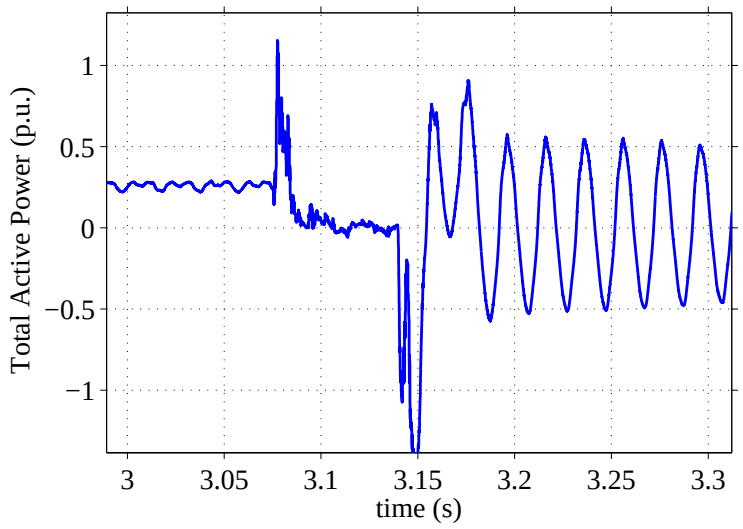

(b) Simulated active power during severe voltage dip.

Figure 5.2: Measured and simulated P_{total} for severe voltage dip.

In summary, while the general response of the detailed model agrees with the field measured response, more research is required to fully validate the detailed model and is included as an area for future work.

5.1 Damping analysis of the DFIG model

In [5], the stability of the DFIG is analyzed. It is noted that in studying the stability of the DFIG mathematically, it can be shown that the DFIG has poorly damped poles around the line frequency, and also that the system becomes unstable when the d component of the rotor current exceeds a certain value. Different methods for damping the flux oscillations are discussed, and it is noted that a comparison is done in [10]. The methods discussed are:

- feedback of the derivative of the flux. This method was shown to work considerably well and at a low cost. The disadvantage concluded from [10] is that it causes relatively high rotor currents.
- introduce a converter connected to the star point of the stator windings, thereby introducing an extra degree of freedom that can be used to damp the flux oscillations. This method works quite well, but has the obvious disadvantage of added hardware, software, and thereby added cost.
- reducing bandwidth of the current controller. This method was shown to work quite well, but compromises the controller's ability to quickly react to grid disturbances, such as voltage drops or overvoltages.
- compensation of the transformation angle to synchronous coordinates. This method was shown to have only a small effect on damping the oscillations.

In this thesis, the DFIG was first modeled without any form of flux damping, followed by an analysis of the poles to determine how best to influence the stability and damping of the system.

Initial simulation results of the DFIG with a current controller in cascade with active power and reactive power controllers show large oscillations close to 50 Hz that are difficult to damp. An analysis was carried out to define the poles that exist due to the interaction between the DFIG machine and current controller. From this analysis, it is made clear the origin of the poles and which parameters influence the poles, leading to a better understanding of how the poles can be damped.

First, the equations of the machine and current controller were developed and state variables identified to allow for state-space implementation. This was done in a similar

manner to the state-space equation 3.11 derived previously. The selected state variables are Ψ_{sd}, Ψ_{sq}, i_{Rd}, i_{Rq}, eI_d, and eI_q, where eI_d and eI_q are the integrated errors, or, the output of the current controller integrator. The input variables are i_{Rd}^{ref}, i_{Rq}^{ref}, and the initial values i_{Rd0}^{ref} and i_{Rq0}^{ref} . From here, the state-space matrix can be derived.

To analyze the poles, damping, and stability of the model, the $pzmap$ (pole-zero map) function in Matlab is utilized. The pole-zero map displays all poles and zeros of the state space equation. Figure 5.3 is a pole-zero map using the base equations described above, with $\alpha_{cc} = 200\pi$ and $R_a = 0$. The model contains four poles, a pole pair near the imaginary axis at around 300 rad/s, and two located on the real axis. Poles can be considered well damped when they lie within lines drawn at 45 degrees from the imaginary axis in both the upper and lower quadrant. Therefore, poles near the real axis are well within these 45 degree lines and are considered very well damped. This analysis will therefore focus on the poorly damped pole pair near the imaginary axis.

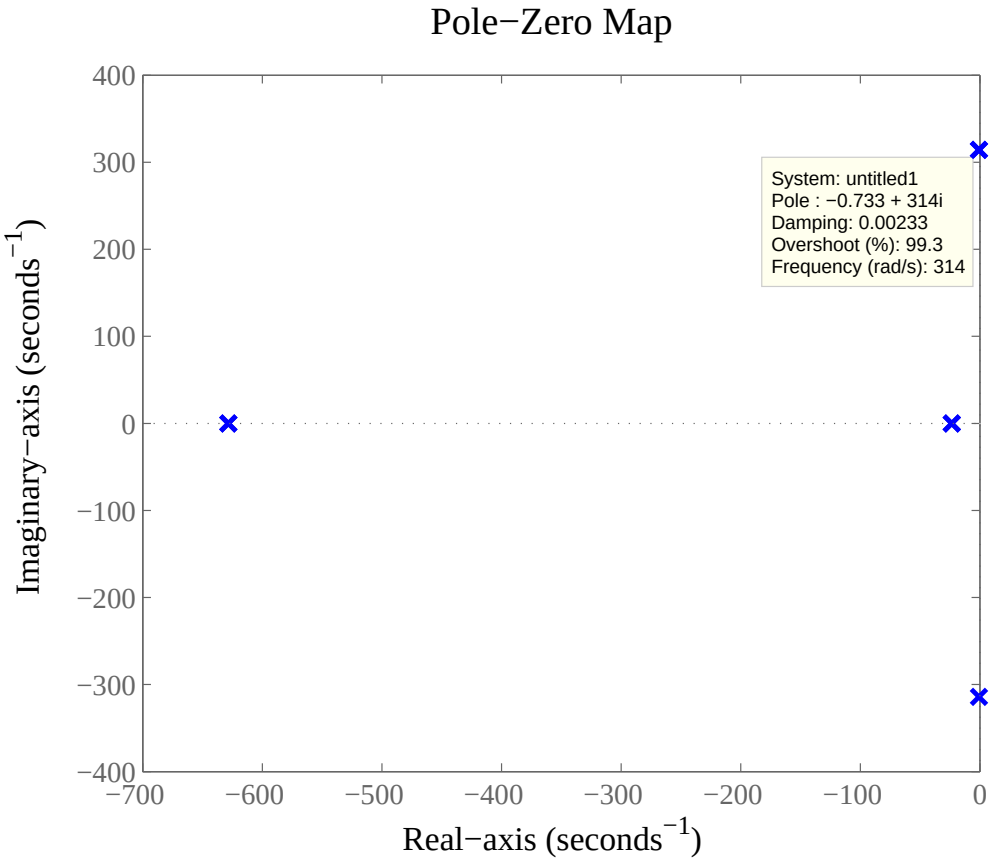

Figure 5.3: Pole-zero map of state-space model for DFIG with PI current controller, with $\alpha_{cc} = 200\pi$ and $R_a = 0$

The two poles at 300 rad/s near the imaginary axis represent the poorly damped poles near 50 Hz that were expected based on the simulation results of the detailed DFIG model. A closer inspection reveals a damping coefficient of 0.00233 for the two poles. It is desirable to move these poles off of the imaginary axis, in the direction of the 45 degree lines that represent well damped poles. With this understanding, the DFIG model parameters can now be modified to see how or if the poles can be moved to increase the damping. The following cases were analyzed:

- With and without the back emf feed forward term
- With and without the active damping term R_a
- Varying values of stator resistance R_s
- Varying values of rotor resistance R_R
- Varying values of magnetizing inductance L_M
- Varying values of stator inductance L_s
- Varying values of stator voltage magnitude U_s
- Varying values of rotor speed ω_r
- Varying values of current controller bandwidth α_{cc}

The results of the analysis show only two parameters having a significant impact on the poorly damped poles, R_s and α_{cc}. Damping increased with increasing stator resistance and with decreasing controller speed, or bandwidth. The stator resistance is obviously not an adjustable parameter, and therefore does not help with damping the poles. Decreasing the bandwidth is not desirable as mentioned above. It is interesting to note that the active damping term R_a did not have a significant impact on the pole damping as expected. Figures 5.4 and 5.5 show the movement of the poles with variation in R_s and α_{cc}. Clearly the simulated values of R_s are not reasonable or practical, but are used here simply to demonstrate the impact on the pole damping.

In [5], the method chosen to damp the stator flux oscillations is through a feedback of the derivative of the flux. This method is chosen due to the low cost (no need for added hardware) and easy implementation. In order to do this, a new component Δi_{Rd}^{ref} is added to the d component of the rotor reference current, as

$$\Delta i_{Rd}^{ref} = \frac{s}{s+\alpha_f}\frac{\alpha_d}{R_s}\psi_s \tag{5.1}$$

where α_d and α_f are flux damping parameters that must be determined. According to [5], the low-pass filter cut-off frequency α_f must be set lower than the frequency of

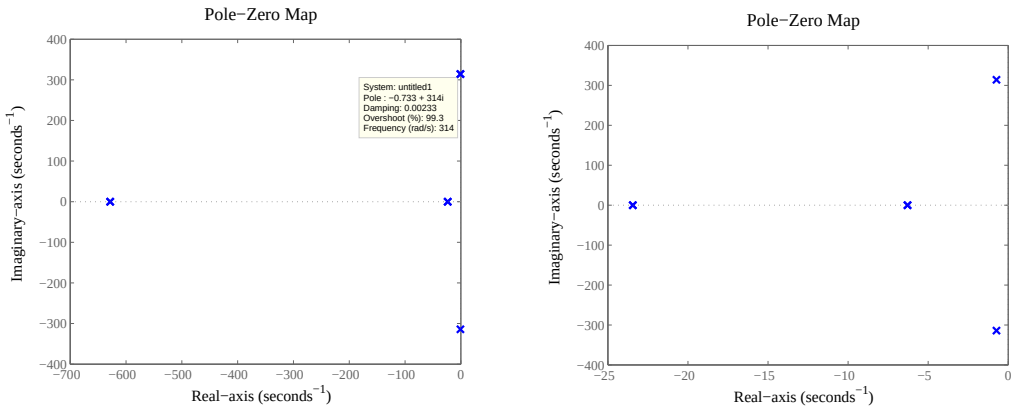

(a) $R_a = 0$ and $\alpha_{cc} = 200\pi$ (b) $R_a = 0$ and $\alpha_{cc} = 2\pi$

Figure 5.4: Pole-zero maps with varying bandwidth of current controller

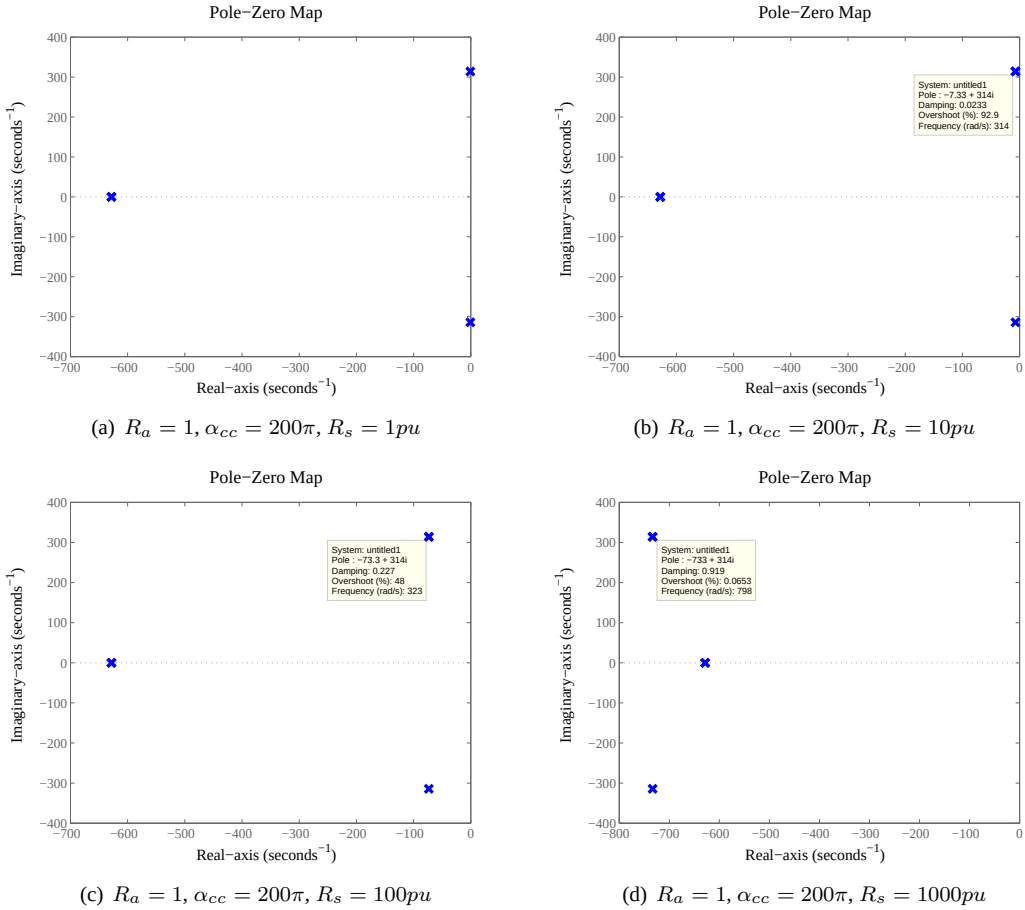

(a) $R_a = 1, \alpha_{cc} = 200\pi, R_s = 1pu$ (b) $R_a = 1, \alpha_{cc} = 200\pi, R_s = 10pu$

(c) $R_a = 1, \alpha_{cc} = 200\pi, R_s = 100pu$ (d) $R_a = 1, \alpha_{cc} = 200\pi, R_s = 1000pu$

Figure 5.5: Pole-zero maps with varying values of stator resistance R_s

the oscillations in order to damp them at all. The damping term α_d must be chosen to be smaller than the current controller bandwidth in order to ensure that the flux damper is slower than the current dynamics. Values of $\alpha_d = 0.7pu$ and $\alpha_f = 0.05pu$ are recommended as initial values. Petersson notes in his analysis of this method that the flux damper shows a high sensitivity to voltage sags, specifically because the Δi_{Rd}^{ref} term must be kept within certain limits to maintain stability. These limits are dependent on both the magnitude of the voltage sag and the α_d term.

For this thesis, the flux damping term was first implemented in the state space representation of the DFIG model to analyze the impact on the poorly damped pole pair. The results of this analysis show the pole pair moving away from the imaginary axis and therefore an increase to the pole damping.

The flux damping term was then implemented in the 5th order transient model in Matlab to verify the results. The flux damper greatly reduces the stator flux oscillations and the active power oscillations prior to the fault. Figure 5.6 shows the stator flux before and after implementation of the flux damping term. In this example, the grid voltage used was actual field measured data, which contained some harmonics and asymmetry, therefore resulting in voltage ”disturbances” being applied to the system. This results in the pre-fault oscillations before the fault occurs near three seconds. Figure 5.6(a) shows how drastic the instability and oscillations are for the undamped model.

However, a few adverse effects are introduced, namely the introduction of harmonics and an increase to the reactive power oscillations. The increase in reactive power oscillations also reduces the controllability of i_{Rd} during the fault and thus affects the active power P during the fault. The root cause of these effects are beyond the scope of this thesis, and is included as an area for future work on this subject.

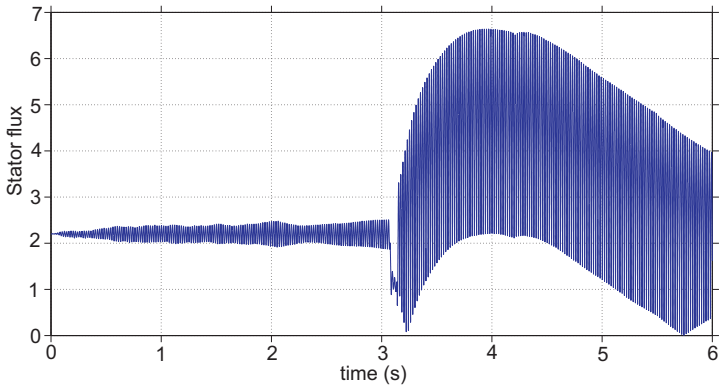

(a) Stator flux without flux damping

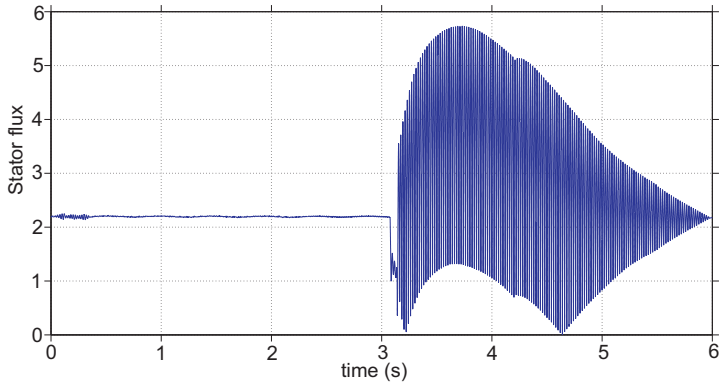

(b) Stator flux with flux damping

Figure 5.6: Stator flux oscillations before and after implementation of flux damping.

Chapter 6

DFIG Simplified Model

The main focus in the development of this simplified model is to reduce the complexity of the model in order to achieve fast simulation times for large network models, while still keeping an acceptable level of accuracy in the characterization of the DFIG machine. The term ”acceptable level”, in the context of this thesis and research, refers to the ability of the model to characterize the active and reactive power response of the DFIG during voltage dips, in order to properly study system level voltage and transient stability. With the PSS/E software used for stability analysis, a typical simulation time step value is 10ms. Therefore many of the simplifications of this model center around the understanding of what/which phenomena can be captured at this granularity, and which phenomena happen ”too quickly” and can therefore be neglected. Another important aspect is understanding the speed and duration of typical voltage dips, and deciding which aspects of the wind turbine model can be captured in this timeframe, and which aspects occur too slowly to be effectively represented.

6.1 Review of simplified DFIG models for stability studies

One of the more common and traditional simplifications of the DFIG machine used in power system stability studies is to model the generator as a negative load. In [11], the Variable Speed Wind Turbine (VSWT) is modeled in this way, with a negative conductance (G) and positive susceptance (B), without differentiation between the DFIG and a Full Power Converter Wind Turbine model. The generator acts as a constant MVA source as long as the current has not reached the limit of either the RSC or GSC. Once the limit is reached, the generator behaves like a constant current source, with varying G and B. This model can be sufficient in simple network analysis with only a few buses, but becomes limited in modeling the DFIG for larger network analyses, as it does not properly

represent the dynamic relationship between the rotor and stator, and the impact of these dynamics on the output P_r, P_s, and Q_s.

A reduced order model in [12] simplifies the fifth-order model down to a third-order model by neglecting stator transients. The model includes enhancements to deal with the various crowbar activation modes for the rotor side converter protection scheme. However the model still includes a current controller which requires a small time step resolution to realize the high bandwidth of the controller.

A simplified model of the DFIG wind turbine is proposed in [13], which neglects both stator and rotor transients and therefore removes all differential equations. The current controller is considered to act instantaneously, meaning $i_r = i_r^{ref}$. The result is a set of 13 algebraic equations which must be solved with an iterative mathematical solver such as the Newton-Raphson method, simultaneously with the network equations. While the model does provide a fundamental frequency model as desired, an iterative solving method is not preferred due to the algebraic loops, and the increased simulation time for larger network models.

In [14], the stator dynamics are again neglected, and the DFIG is simplified to a voltage behind a transient reactance. Algebraic loops are avoided by introducing a time lag in the current controller. This model does include the torsional relationship between the wind turbine shaft and generator rotor, and therefore a two-mass shaft model is included. The model does not account for current limitation of the RSC, and does not include a clear FRT algorithm. The model includes a pitch controller and accounts for the changes in wind speed with respect to the mechanical power, or torque, input.

In both [15] and [16], GE wind turbines are modeled as controlled current sources. Rotor quantities are omitted, which neglects the relationship between the controlled rotor voltages and the stator side variables, which may compromise the accuracy of the results for output active and reactive power under certain conditions. This model does not account for the fault ride-through process and neglects the current limitations of the RSC.

6.2 List of Model Simplifications

Several simplifications of the detailed model were analyzed for this thesis. The simplifications will be modeled and discussed, step by step, moving from the original 5th order machine model with P and Q controllers, to the final simplified model intended for PSS/E implementation. The simplifications to be discussed in the following sections are as follows:

1. Comparison of the 5th order machine model with current controller and outer loop P and Q controllers, to a 3rd order model in which the stator flux dynamics are

removed.

2. Comparison of the 3rd order machine model with current controller and outer loop P and Q controllers, to a 2nd order model where the rotor speed is fixed.

3. Comparison of the 2nd order machine model with current controller and outer loop P and Q controllers with a fixed rotor speed, to the final simplified model, which removes the machine model and instead represents the system as a set of algebraic equations. The P and Q controllers are still in place with this model.

In all of the following model comparisons, each model was simulated against a synthetic voltage profile, with a pre-fault value of 1.0 p.u., and a voltage drop occurring at 1s for a duration of 250 ms. The simulations were compared for voltage drop values of 0.8 p.u. and 0.25 p.u., where the voltage drop value represents the per unit value of the remaining voltage during the drop. The base test case for each comparison is for an operating point at rated power, or super-synchronous operation. Operating points at synchronous speed and sub-synchronous speed were also modeled and results can be found in the Appendix. For the purposes of illustration, active power and reactive power are shown to be positive when injecting power into the grid (this convention is opposite to the actual machine model in which positive power is consumed by the machine).

6.3 Comparison of 5th order machine model to 3rd order machine model

The first simplification made to the detailed DFIG model is the elimination of the stator flux dynamics, or $\frac{d\underline{\Psi}_s}{dt} = 0$. The machine model used in this thesis represents the rotor and stator flux as the state variables. Therefore, by eliminating the time dependent portion of the stator flux, two states are eliminated (Ψ_{sd} and Ψ_{sq}) and the model is reduced from a 5th order to a 3rd order. The elimination of the stator flux dynamics will also remove the $\sim$50 Hz oscillations, as it was shown in previous sections that the poorly damped poles are due to the stator flux.

Figures 6.1 through 6.2 show a comparison between the 5th order model and the 3rd order model. As the aim of this thesis is to develop simplified models for voltage and transient stability, the key variables to study are the active and reactive powers that interact with the power system. Therefore moving forward only P_{total} and Q_s will be discussed. Results comparing other machine variables and for various voltage dip magnitudes can be found in the Appendix.

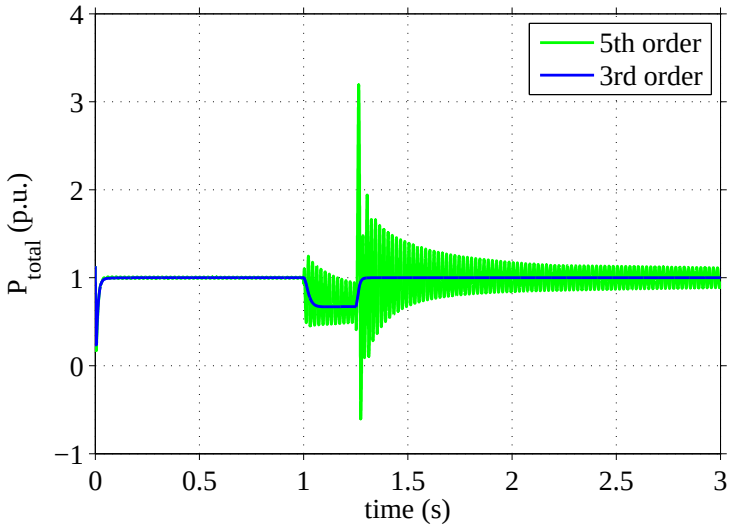

(a) P_{total} comparison of 5th and 3rd order models

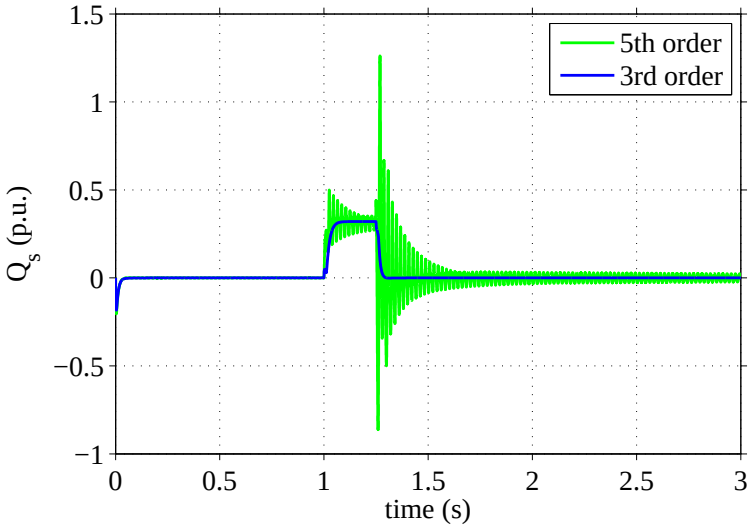

(b) Q_s comparison of 5th and 3rd order models

Figure 6.1: P_{total} and Q_s 5th and 3rd order models, super synchronous operation, 0.8 p.u. voltage dip.

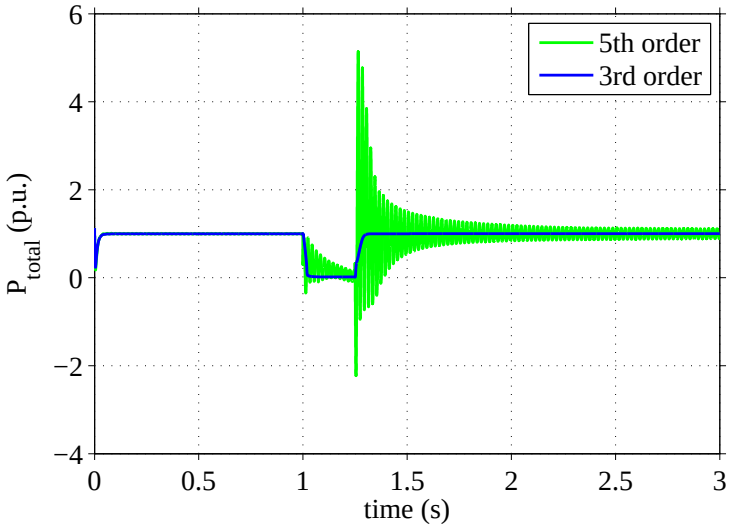

(a) P_{total} comparison of 5th and 3rd order models

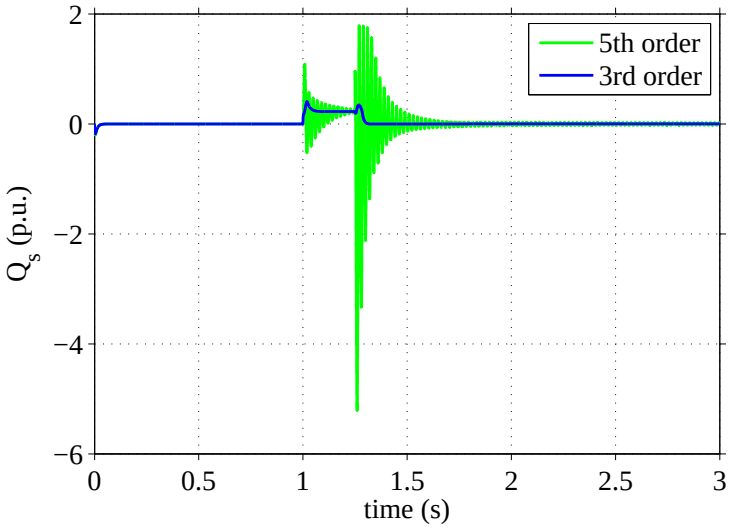

(b) Q_s comparison of 5th and 3rd order models

Figure 6.2: P_{total} and Q_s 5th and 3rd order models, super synchronous operation, 0.25 p.u. voltage dip.

6.4 Comparison of 3rd order machine model to 2nd order machine model

The next simplification made to the machine model is to assume the rotor speed is fixed, or $\frac{d\omega_r}{dt} = 0$, resulting in a 2nd order machine model. This simplification is based on the assumption that the time period of interest during a voltage dip is fast compared to the rotor speed dynamics. In other words, it is assumed that the voltage dip occurs, and is subsequently removed from the system, in a short enough period of time that will not cause a substantial change in rotor speed. In the interest of this thesis, it is not the actual change in rotor speed that is of importance, but rather the effect of the rotor speed dynamics on the overall active and reactive power output from the DFIG during the transient event. Figures 6.3 and 6.4 show the P and Q response during super synchronous operation, for both a shallow and severe voltage dip. The results indicate no substantial change to the P and Q by assuming the rotor speed is fixed.

The Appendix contains figures for a broader range of operating points, voltage dips, and other variables of interest, including the actual change in ω_r. The results show the rotor speed continuing to increase after the fault is cleared from the system. In reality, the speed would be controlled to its reference value by pitching the rotor blades and thereby decreasing the input mechanical power. The rotor speed would then decelerate back to the reference speed. In order to simulate this, a slow outer loop speed controller can be implemented in the model.

6.5 Development of the final simplified DFIG model

The final simplification made to the DFIG model is based on an understanding of the final simplified model intended for use in PSS/E. As previously mentioned, the time step is typically 10 ms. This small of a time step limits what the simplified model will be able to capture and represent. If it is assumed that 10 measuring points are needed to properly capture a sinusoidal curve, then a model with a 10 ms time step will be limited to capturing frequencies greater than 10 Hz. Therefore, the 50 Hz oscillations previously illustrated in the 5th order detailed DFIG model will not be captured by a model implemented in PSS/E at 10 ms time steps.

Based on this, the final assumption is that the action of the current controller is very fast relative to the simulation time step. This leads to the final simplification:

1. The rotor current is equal to the rotor current reference value, and therefore the current controller is omitted from the model.

The following is a summary of simplifications made to the base detailed DFIG model:

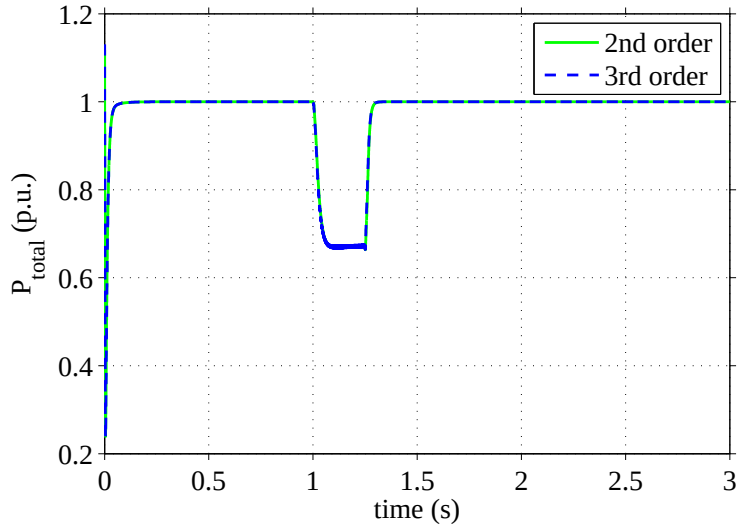

(a) P_{total} comparison of 3rd and 2nd order models

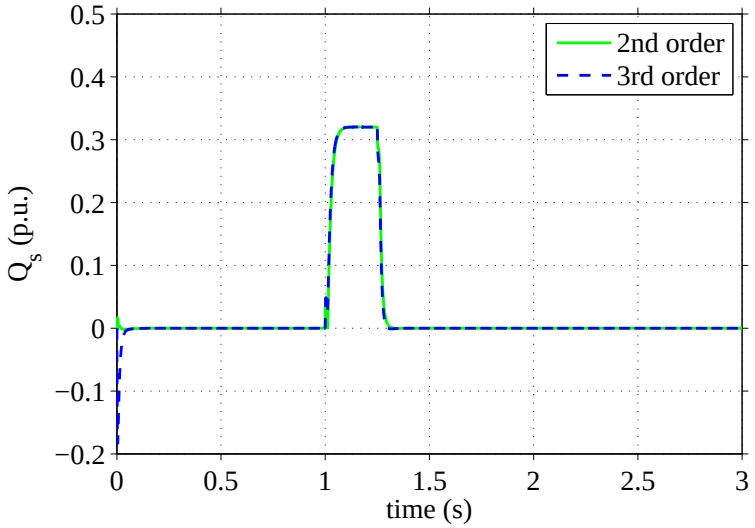

(b) Q_s comparison of 3rd and 2nd order models

Figure 6.3: P_{total} and Q_s 3rd and 2nd order models, super synchronous operation, 0.8 p.u. voltage dip.

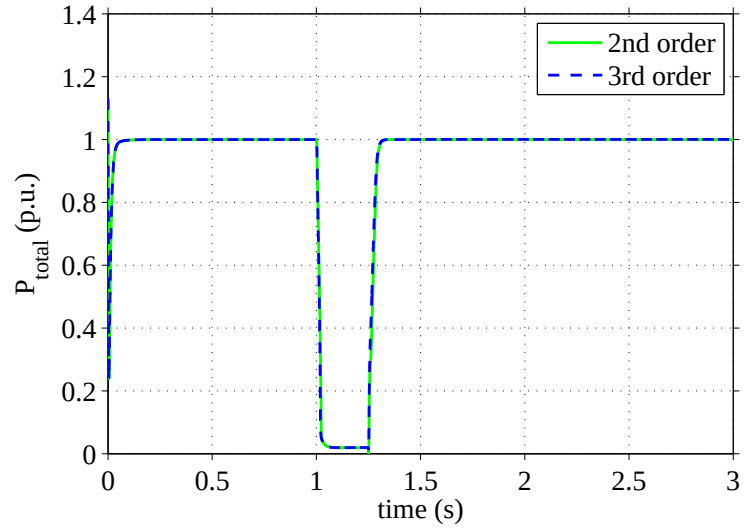

(a) P_{total} comparison of 3rd and 2nd order models

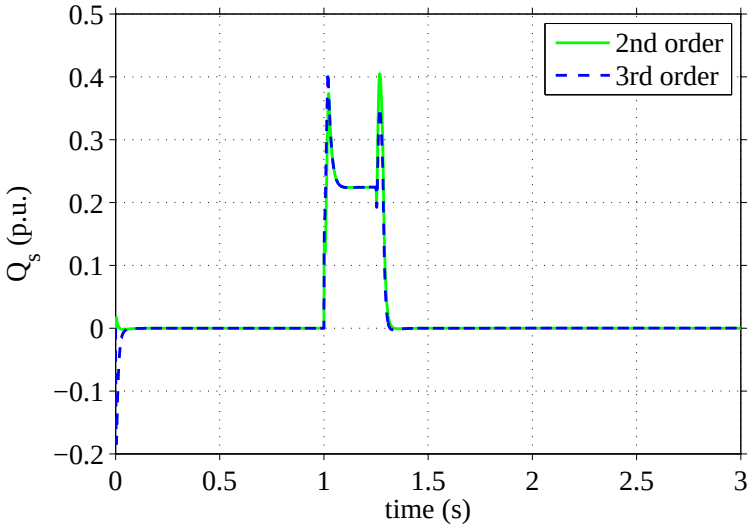

(b) Q_s comparison of 3rd and 2nd order models

Figure 6.4: P_{total} and Q_s 3rd and 2nd order models, super synchronous operation, 0.25 p.u. voltage dip.

1. The rotor and stator transients are neglected. Therefore $\frac{d\underline{\Psi}_r}{dt}$ and $\frac{d\underline{\Psi}_s}{dt} = 0$.
2. The rotor speed is considered to be constant, as the time period of interest during voltage dips and stability analysis is fast relative to the rotor speed dynamics.
3. The mechanical torque T_m is considered constant over the time period of interest. Similar to the previous simplification, the dynamics of the wind speed and thus input mechanical torque is slow compared to the electrical dynamics of the machine.
4. The current controller has been omitted, as the action of the current controller is considered to be instantaneous.

With these simplifications, equation (3.1) can be simplified to the following:

$$\underline{u}_r = R_r\underline{i}_r + j(\omega_s - \omega_r)\underline{\Psi}_r \tag{6.1}$$

and inserting equation (3.4) into (6.1), yields

$$\begin{aligned} \underline{u}_r &= R_r\underline{i}_r + j(\omega_s - \omega_r)(L_m\underline{i}_s + L_r\underline{i}_r) \\ &= R_r\underline{i}_r + j(\omega_s - \omega_r)L_m\underline{i}_s + j(\omega_s - \omega_r)L_r\underline{i}_r \\ &= R_r\underline{i}_r + jsX_m\underline{i}_s + jsX_r\underline{i}_r \end{aligned} \tag{6.2}$$

where

$$\begin{aligned} X_m &= \omega_s L_m \\ X_r &= \omega_s L_r \\ X_s &= \omega_s L_s \\ s &= slip = \frac{\omega_s - \omega_r}{\omega_s} \end{aligned}$$

Equation (3.1) can also be simplified, using (3.3), as follows:

$$\begin{aligned} \underline{u}_s &= R_s\underline{i}_s + j\omega_s\underline{\Psi}_s \\ &= R_s\underline{i}_s + j\omega_s(L_s\underline{i}_s + L_m\underline{i}_r) \\ &= \underline{i}_s(R_s + j\omega_s L_s) + j\omega_s L_m\underline{i}_r \end{aligned} \tag{6.3}$$

yielding an equation that can be used to solve for $\underline{i}_s$ as:

$$\begin{aligned} \underline{i}_s &= \frac{\underline{u}_s - j\omega_s L_m \underline{i}_r}{R_s + j\omega_s L_s} \\ &= \frac{\underline{u}_s - jX_m \underline{i}_r}{R_s + jX_s} \end{aligned} \tag{6.4}$$

The simplified model is therefore represented by the previously defined set of algebraic equations, with an outer P controller and an outer Q controller designed to provide reactive power support per the E.ON grid code. Figure 6.5 represents a simplified control diagram of the original 5th order machine model with current controller and outer P and Q controllers, followed by the simplifications made in arriving at the final simplified model control diagram.

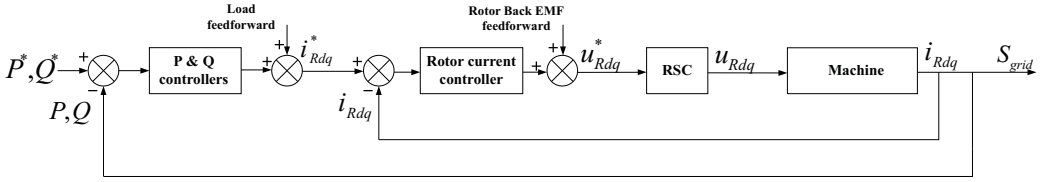

(a) Original control diagram of 5th order machine model with current controller and outer P and Q controllers

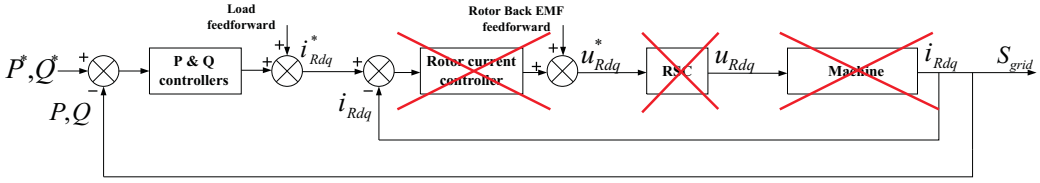

(b) Simplifications made for final simplified model

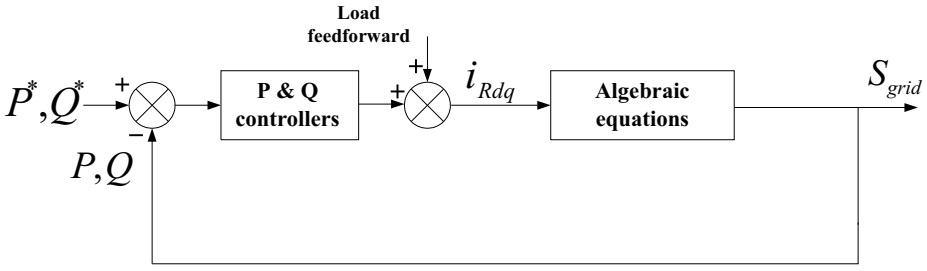

(c) Final simplified model

Figure 6.5: Original detailed model control diagram and final simplified model

6.6 Comparison of 2nd order machine model to machine modeled as a set of algebraic equations

The final simplified model as described in the previous section is compared to the 2nd order machine model. For this discussion, the final simplified model will be referred to

as just the 'simplified' model. Figures 6.6 and 6.7 illustrate the two models for super synchronous operation, with voltage dips of 0.8 p.u. and 0.25 p.u., respectively. P_{total} and Q_s are the only variables shown, with further documentation found in the Appendix.

The results of the comparison show good agreement between the two models. As expected, the simplified model is not able to identify the transients that occur at the beginning and end of the voltage dip. The reactive power and active power show near perfect agreement. This results in the conclusion that the simplified model is able to accurately demonstrate the trend of the active and reactive power as compared to the detailed 5th order model.

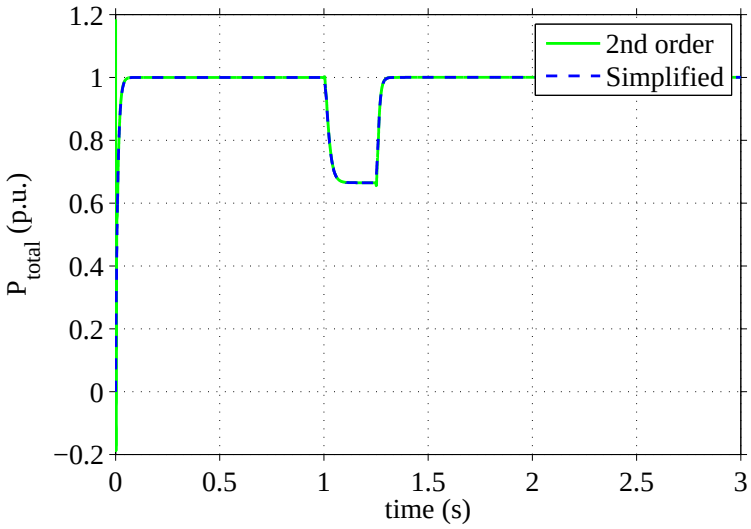

(a) P_{total} comparison of 2nd order and simplified models

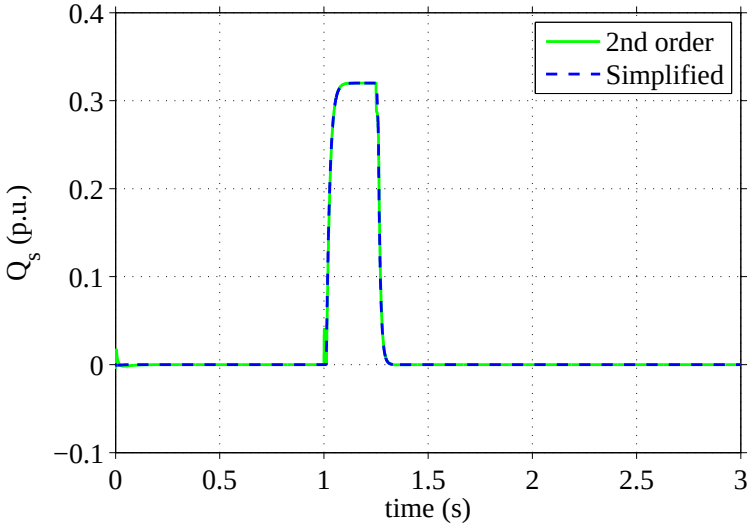

(b) Q_s comparison of 2nd order and simplified models

Figure 6.6: P_{total} and Q_s 2nd order and simplified models, super synchronous operation, 0.8 p.u. voltage dip.

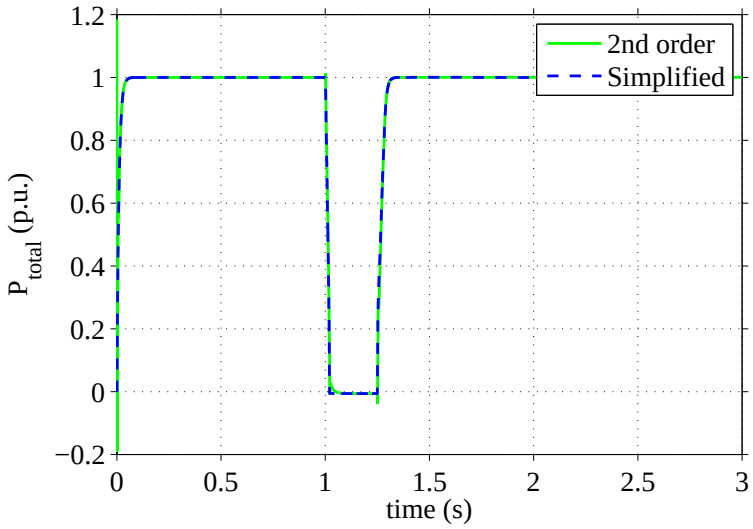

(a) P_{total} comparison of 2nd order and simplified models

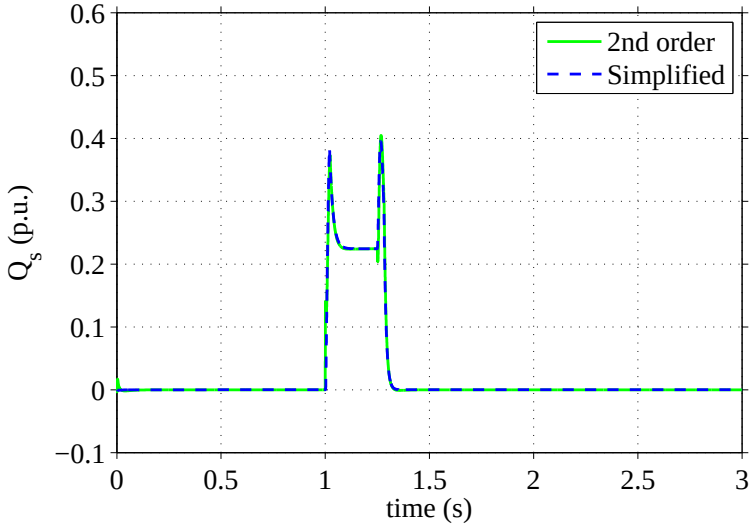

(b) Q_s comparison of 2nd order and simplified models

Figure 6.7: P_{total} and Q_s 2nd order and simplified models, super synchronous operation, 0.25 p.u. voltage dip.

Chapter 7

Conclusions and Future Work

7.1 Conclusions

The aim of this work was to develop a simplified model for the DFIG wind turbine for power system stability studies with an emphasis on short-term voltage stability analyses. A detailed model of the DFIG was developed, and was compared to field measurements. Several simplifications to the detailed model were investigated and compared with the detailed model.

Investigation of DC-chopper

The DC-chopper operation was analyzed. A simplified representation of the DC-chopper was implemented in the detailed DFIG model. The DC-chopper is modeled by switching the converter operation to a diode rectifier when $|i_r| > i_{r,max}$. In this operation, the rotor voltage $\underline{u_r}$ magnitude is determined by the DC-link voltage, and is in phase with the rotor current. The results demonstrate the general response of the DFIG during diode rectifier operation to be similar to the response without the diode rectifier. For this reason, the DC-chopper operation is not included in the subsequent simplified models.

Comparison to field measurements

The DFIG 5th order machine model with P and Q controllers is compared to a field measured response of a DFIG to a severe voltage dip. The model is found to have reasonable agreement with the general response, however there are significant differences that require further investigation.

Analysis of poorly damped poles of DFIG

The DFIG with current controller configuration is recognized as having poorly damped poles near line frequency (50 Hz). The poles are identified as being associated with the stator flux. The poles are dependent in large part on the bandwidth of the current controller and the stator resistance. Damping is improved by decreasing α_{cc} or by increasing R_s. Further damping efforts are investigated by implementing a stator flux damping term that is discussed in [5], which implements a feedback of the derivative of the flux. The method successfully damps the stator flux oscillations and active power oscillations, however it introduces a few adverse effects including harmonics and higher reactive power oscillations. In [5], it is noted that this method has a high sensitivity to voltage sags. Further analysis of the flux damping methods is left for future work.

Development of simplified models

Simplified models were developed in discrete steps, starting with the 5th order detailed model. The simplifications and conclusions are as follows:

- Stator flux dynamics are neglected, or $\frac{d\underline{\Psi}_s}{dt} = 0$, resulting in a 3rd order machine model. The stator flux oscillations are removed, resulting in a more general response. A comparison to the 5th order model shows the 3rd order model to follow the average 5th order response. The simplification loses some information regarding the high transient oscillations at the beginning of the voltage dip and at fault clearing.

- Rotor speed is fixed, or $\frac{d\omega_r}{dt} = 0$, resulting in a 2nd order machine model. The 2nd order model is compared to the 3rd order model. Although there is a change in ω_r in the 3rd order model, there is not a significant impact to the P and Q response as compared to the 2nd order model.

- The action of the current controller is considered to be instantaneous, and therefore the current controller is omitted from the model. This results in the machine model being omitted as well, and instead representing the machine variables by a set of algebraic equations. The final simplified model is therefore a 0 order machine model with P and Q controllers, see Figure 7.1. The final simplified model is compared to the 2nd order model with near perfect agreement. It is concluded that the final simplified model is an accurate representation of the general P and Q response of the DFIG.

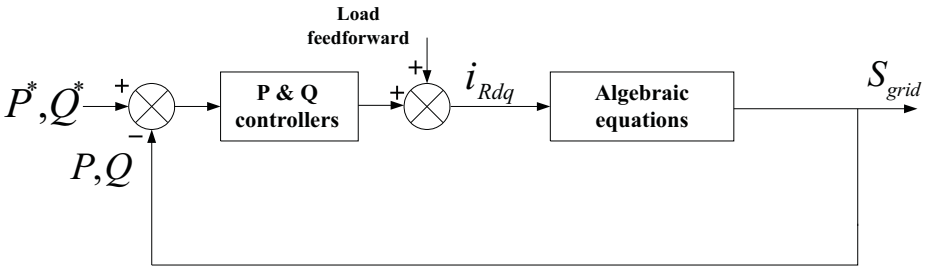

Figure 7.1: Final simplified model

7.2 Future work

In the development of the detailed DFIG model, several topics are of interest for further development and research. The proposed areas for future work are:

- Validation of the detailed model to field measurements requires more research. Although the PSCAD model has been validated against field measurements, the Matlab/Simulink model requires validation in order to validate the use of the subsequent development of the simplified models. One area of interest is the damping of the poorly damped poles of the DFIG.
- Validation of the simplified crowbar/rectifier representation against field measurements, specifically for the purposes of assessing the impact to overall energy balance. For the purposes of this research, it is not necessary to validate the crowbar operation itself, but simply ensure that the model properly represents the effect of the P and Q interaction with the power grid.
- Implementation of the simplified model in PSS/E software.
- Implementation of other grid code requirements in the simplified model.
- Implementation of the simplified model in other positive-sequence phase time-domain dynamic simulation tools, such as DigSilent and PSLF (Power System Utility Software, designed by GE Power Systems).
- Validation of the simplified model against various wind turbine models/manufacturers, with the goal of creating a generic simplified model for use on voltage and transient stability analyses.

References

[1] M. Bongiorno and T. Thiringer, "A generic DFIG model for voltage dip ride-through analysis," *IEEE Transactions on Energy Conversion*, Submitted March 2012.

[2] "World market for wind turbines recovers and sets a new record: 42 GW of new capacity in 2011, worldwide total capacity at 239 GW." Feb 07, 2012. Accessible from: http://www.windea.org, accessed May 01, 2012.

[3] "Renewables 2011 Global Status Report." Published by Renewable Energy Policy Network for the 21st Century, 2011. Accessible from: www.ren21.net.

[4] M. A. Bahmani, "Core loss calculation in amorphous high frequency high power transformers with different topologies," Master's thesis, CHALMERS UNIVERSITY OF TECHNOLOGY, 2011.

[5] A. Petersson, *Analysis, Modeling, and Control of Doubly-Fed Induction Generators for Wind Turbines*. PhD thesis, Department of Energy and Environment Chalmers University of Technology, 2003.

[6] A. Perdana, *Dynamic Models of Wind Turbines, A contribution towards the Establishment of Standardized Models of Wind Turbines for Power System Stability Studies*. PhD thesis, Department of Energy and Environment Chalmers University of Technology, 2008.

[7] J. Fletcher and J. Yang, *Introduction to the Doubly-Fed Induction Generator For Wind Power Applications, Paths to Sustainable Energy, Dr Artie Ng (Ed.)*. InTech, available at: http://www.intechopen.com/books/paths-to-sustainable-energy/introduction-to-the-doubly-fed-induction-generator-for-wind-power-applications, 2010.

[8] T. Thiringer, J. Paixao, and M. Bongiorno, "Monitoring of the ride-through ability of a 2mw wind turbine in tvååker, halland," tech. rep., Elforsk rapport 09:26, Stockholm, Sweden, 2009.

[9] N. Mohan, T. Undeland, and W. Robbins, *Power electronics converters, applications, and design*. Wiley, 2 edition, 1995.

[10] C.R.Kebler, *Aktive dämpfung der doppelt-gespeisten Drehstrommaschine*. PhD thesis, Technishen Universität Carolo-Wilhelmina, 2000(in German).

[11] N. Ullah and T. Thiringer, "Variable speed wind turbines for power system stability enhancement," *IEEE Transactions on Energy Conversion*, Vol.22, No.1, March 2007.

[12] I. Erlich, J. Kretschmann, J. Fortmann, S. Mueller-Engelhardt, and H. Wrede, "Modeling of wind turbines based on doubly-fed induction generators for power system stability studies," Vol.22, No.3, August 2007.

[13] P. Ledesma and J. Usaola, "Doubly fed induction generator model for transient stability analysis," *IEEE Transactions on Energy Conversion*, Vol.20, No.2, June 2005.

[14] Y. Lei, A. Mullane, G. Lightbody, and R. Yacamini, "Modeling of the wind turbine with a doubly fed induction generator for grid integration studies," *IEEE Transactions on Energy Conversion*, Vol.21, No.1, March 2006.

[15] K. Clark, N. Miller, W. Price, and J. Sanchez-Gasca, "Modeling of GE wind turbine-generators for grid studies," tech. rep., General Electric International, Inc., Jan. 2008.

[16] N. Miller, J. Sanchez-Gasca, W. Price, and R. Delmerico, "Dynamic modeling of GE 1.5 and 3.6 MW wind turbine-generators for stability simulations," *Proceeding of Power Engineering Society General Meeting*, vol.3, July 2003, pp. 1977 - 1983.

Appendix A

Results from comparison of model simplifications

The appendix contains results from the comparison of various model simplifications. It includes results from various operating points, voltage dips, or machine variables not shown in the main document. Each section is dedicated to a separate model comparison.

A.1 Comparison of 5th order model to 3rd order model

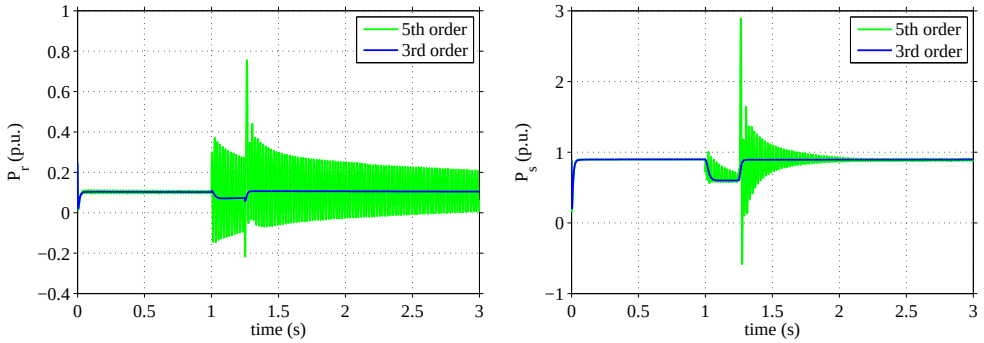

(a) P_r comparison of 5th and 3rd order models

(b) P_s comparison of 5th and 3rd order models

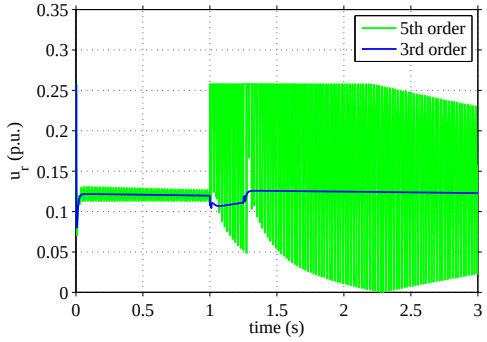

(c) u_r comparison of 5th and 3rd order models

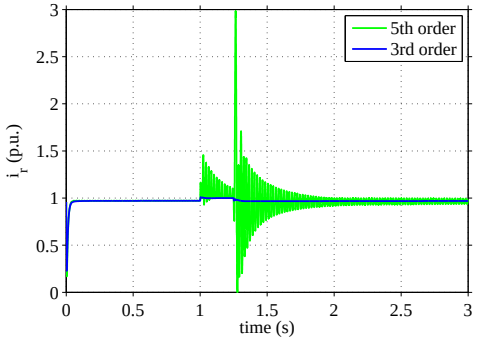

(d) i_r comparison of 5th and 3rd order models

Figure A.1: Comparison of 5th and 3rd order models, super synchronous operation, 0.8 p.u. voltage dip.

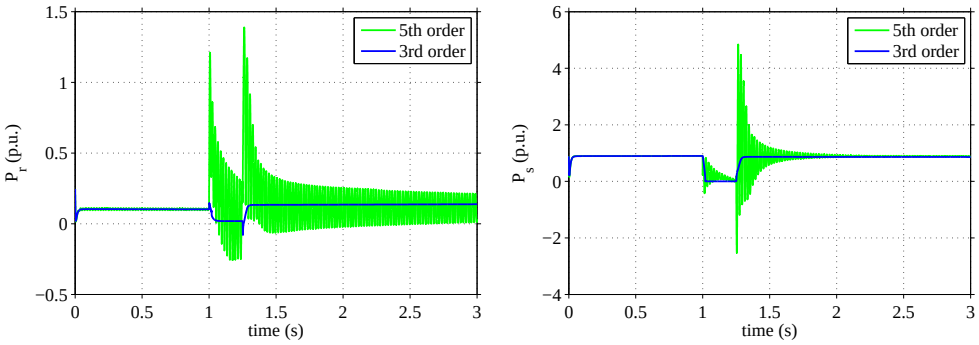

(a) P_r comparison of 5th and 3rd order models

(b) P_s comparison of 5th and 3rd order models

(c) u_r comparison of 5th and 3rd order models

(d) i_r comparison of 5th and 3rd order models

Figure A.2: Comparison of 5th and 3rd order models, super synchronous operation, 0.25 p.u. voltage dip.

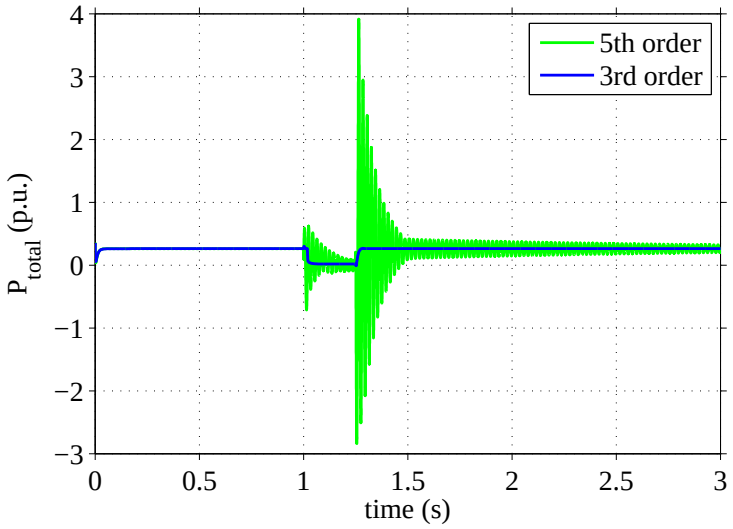

(a) P_{total} comparison of 5th and 3rd order models

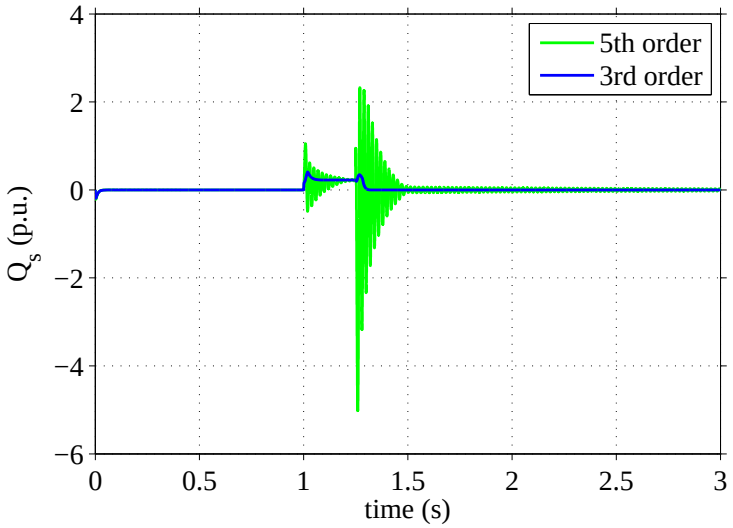

(b) Q_s comparison of 5th and 3rd order models

Figure A.3: P_{total} and Q_s 5th and 3rd order models, synchronous operation, 0.25 p.u. voltage dip.

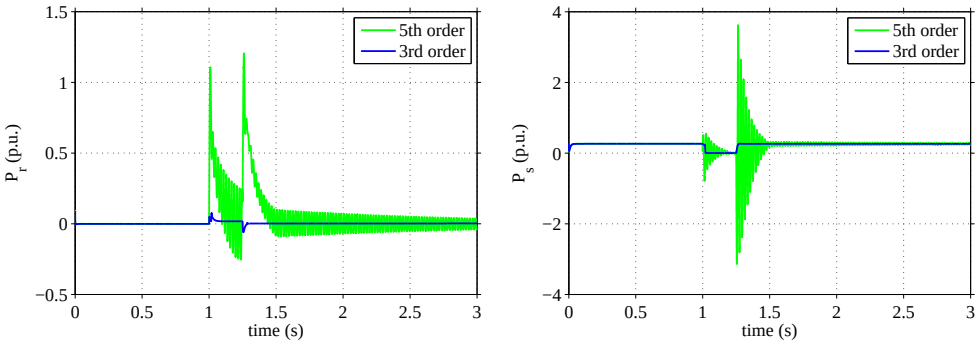

(a) P_r comparison of 5th and 3rd order models

(b) P_s comparison of 5th and 3rd order models

(c) u_r comparison of 5th and 3rd order models

(d) i_r comparison of 5th and 3rd order models

Figure A.4: Comparison of 5th and 3rd order models, synchronous operation, 0.25 p.u. voltage dip.

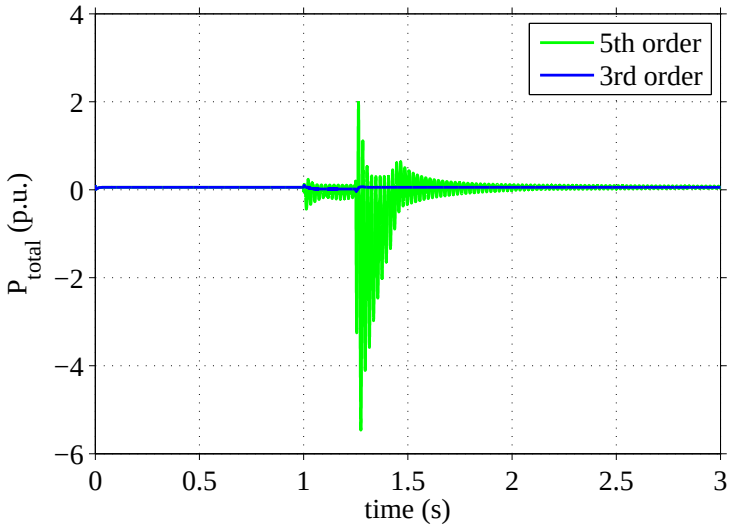

(a) P_{total} comparison of 5th and 3rd order models

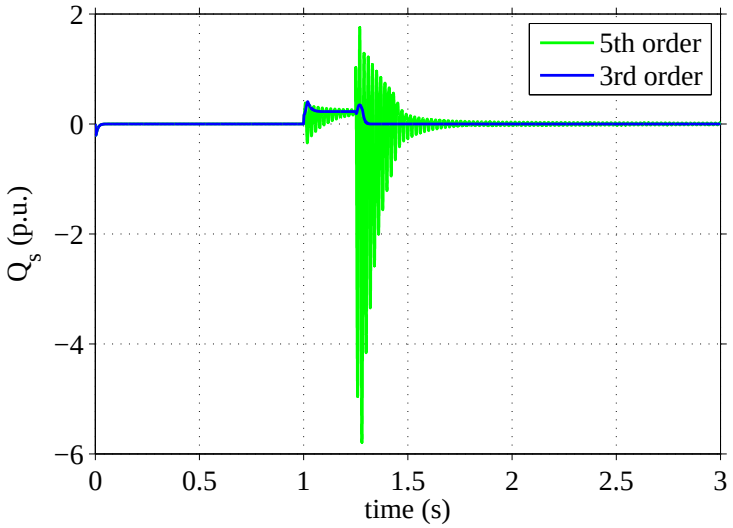

(b) Q_s comparison of 5th and 3rd order models

Figure A.5: P_{total} and Q_s 5th and 3rd order models, sub-synchronous operation, 0.25 p.u. voltage dip.

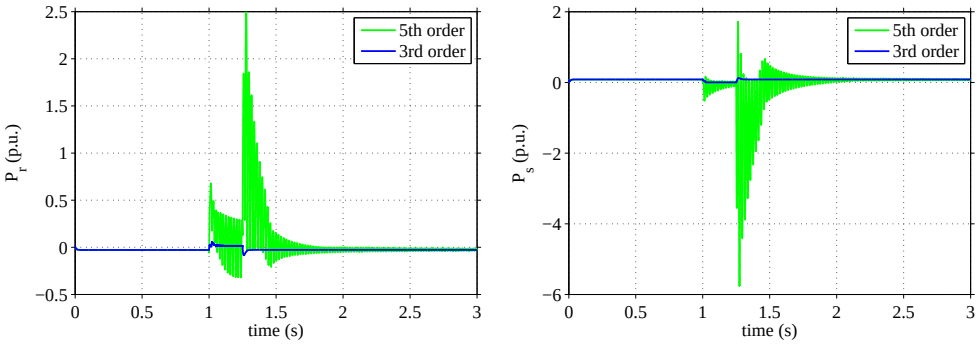

(a) P_r comparison of 5th and 3rd order models

(b) P_s comparison of 5th and 3rd order models

(c) u_r comparison of 5th and 3rd order models

(d) i_r comparison of 5th and 3rd order models

Figure A.6: Comparison of 5th and 3rd order models, sub-synchronous operation, 0.25 p.u. voltage dip.

A.2 Comparison of 3rd order model to 2nd order model

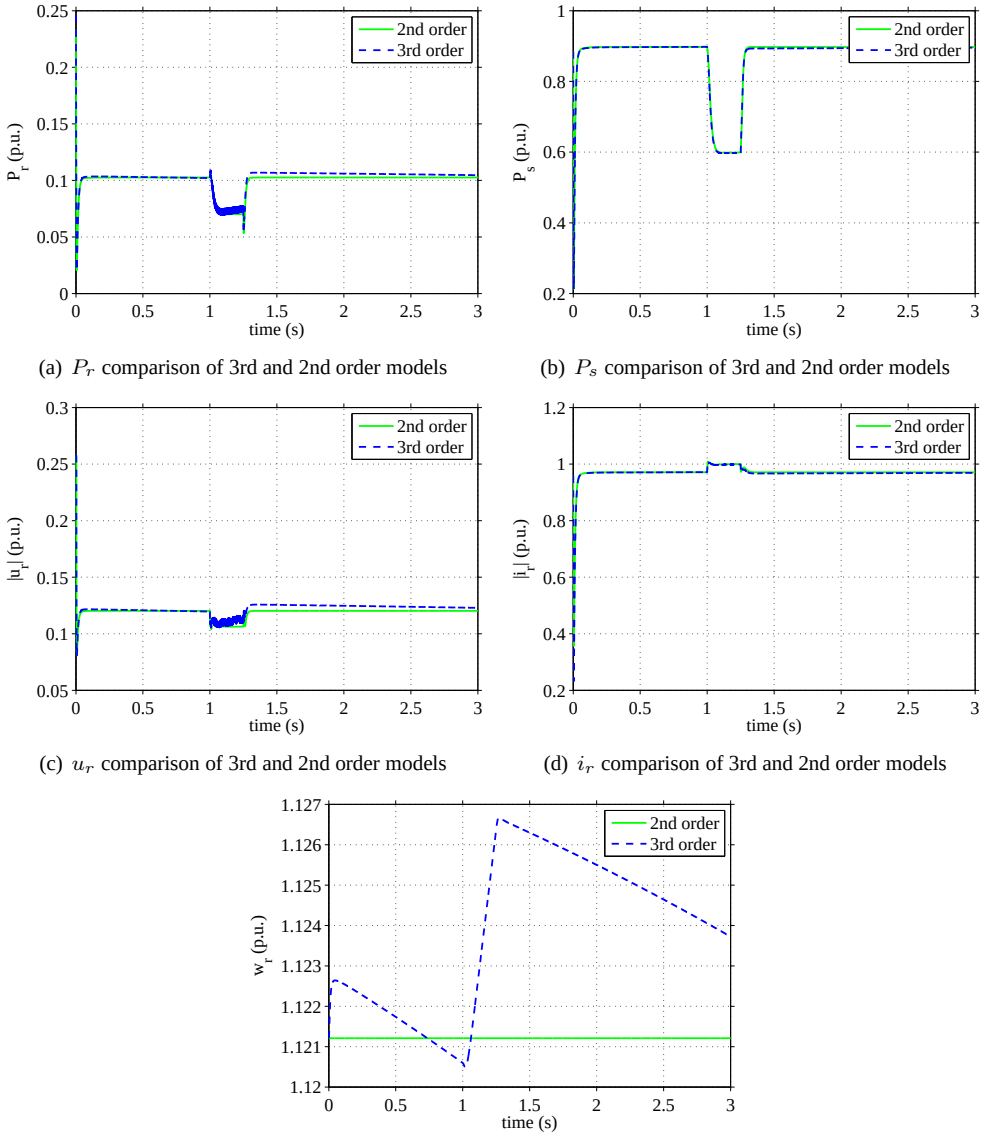

(a) P_r comparison of 3rd and 2nd order models

(b) P_s comparison of 3rd and 2nd order models

(c) u_r comparison of 3rd and 2nd order models

(d) i_r comparison of 3rd and 2nd order models

(e) w_r comparison of 3rd and 2nd order models

Figure A.7: Comparison of 3rd and 2nd order models, super synchronous operation, 0.8 p.u. voltage dip.

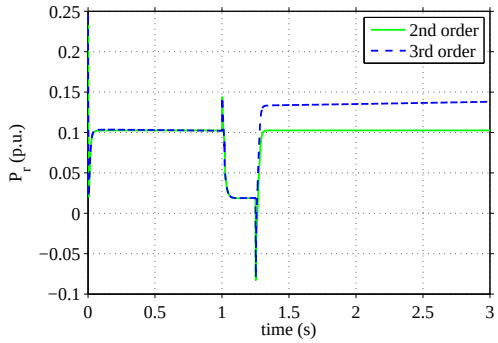

(a) P_r comparison of 3rd and 2nd order models

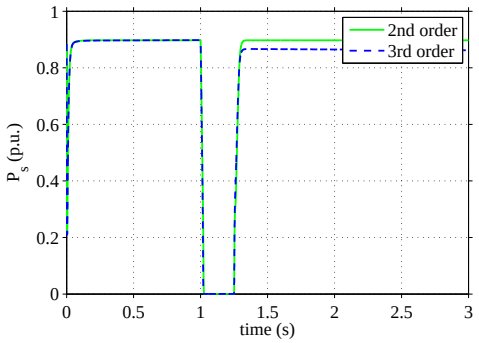

(b) P_s comparison of 3rd and 2nd order models

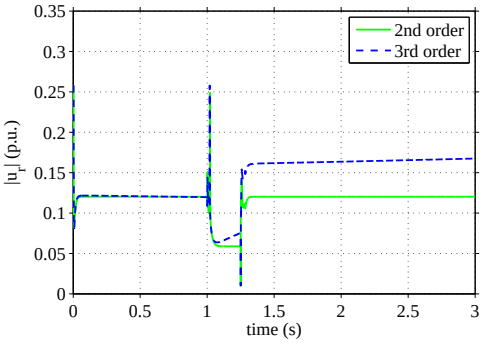

(c) u_r comparison of 3rd and 2nd order models

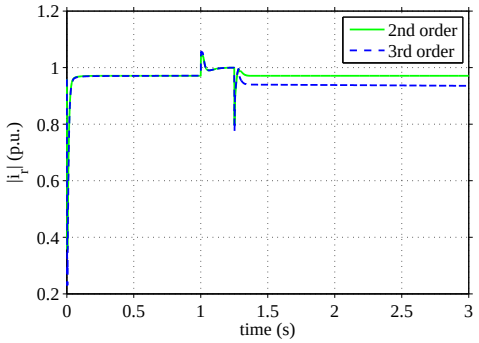

(d) i_r comparison of 3rd and 2nd order models

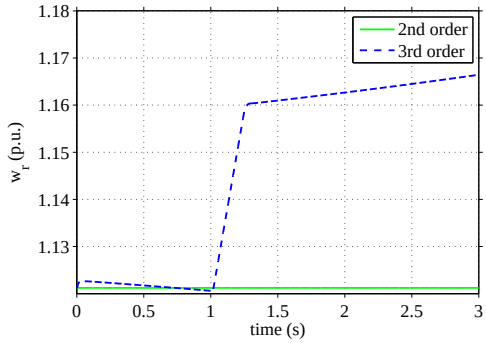

(e) w_r comparison of 3rd and 2nd order models

Figure A.8: Comparison of 3rd and 2nd order models, super synchronous operation, 0.25 p.u. voltage dip.

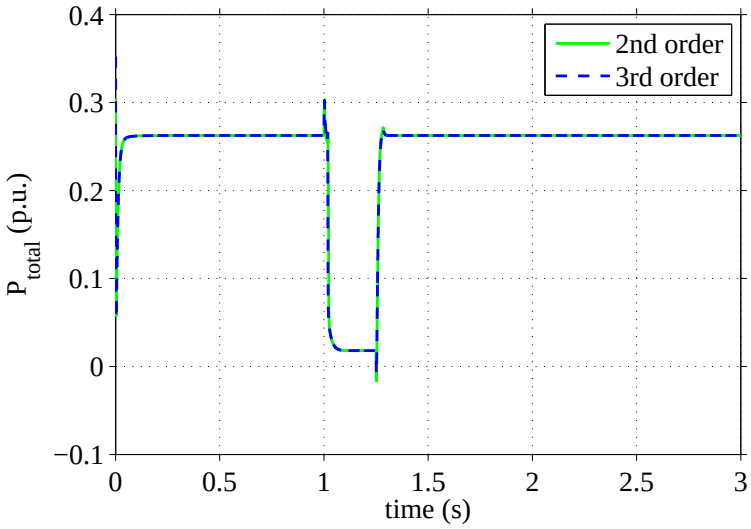

(a) P_{total} comparison of 3rd and 2nd order models

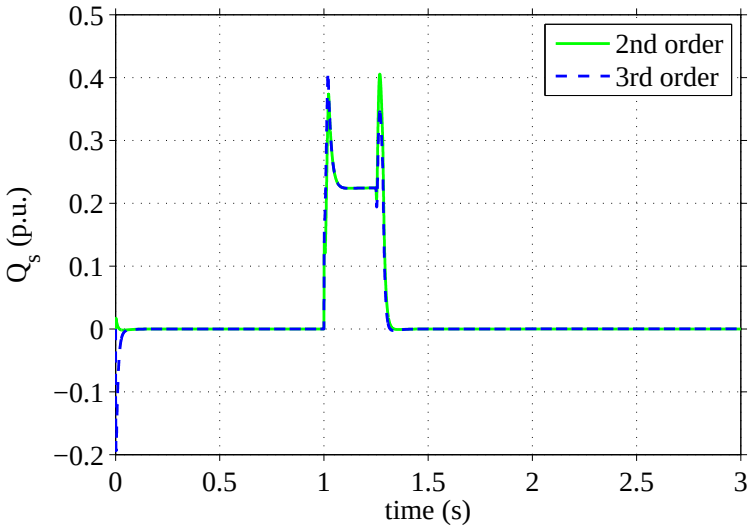

(b) Q_s comparison of 3rd and 2nd order models

Figure A.9: P_{total} and Q_s comparison of 3rd and 2nd order models, synchronous operation, 0.25 p.u. voltage dip.

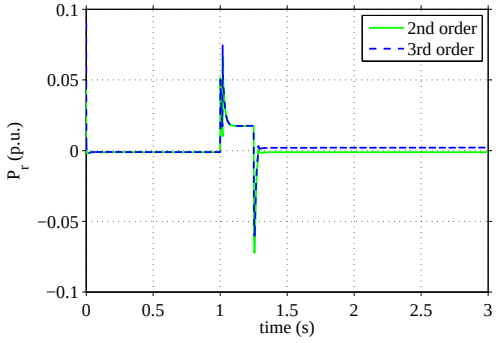

(a) P_r comparison of 3rd and 2nd order models

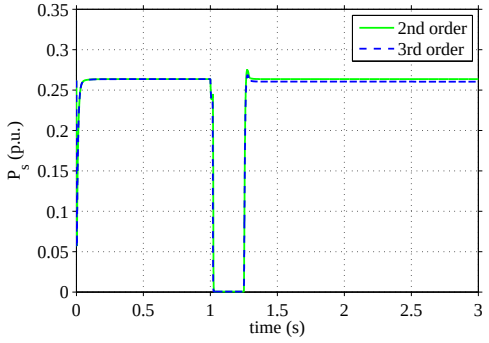

(b) P_s comparison of 3rd and 2nd order models

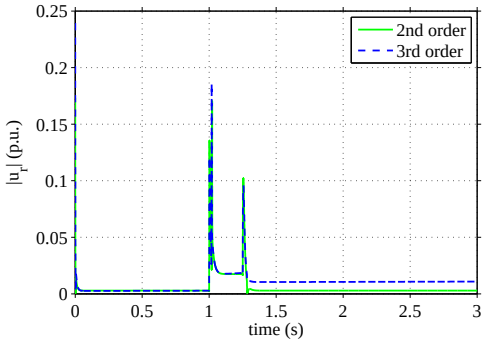

(c) u_r comparison of 3rd and 2nd order models

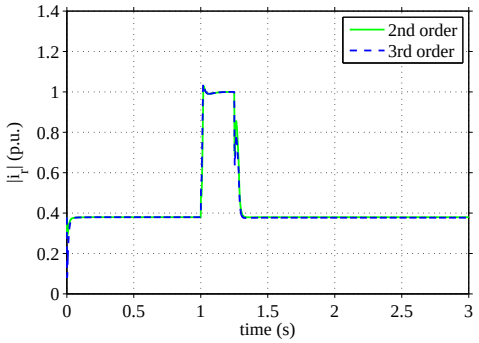

(d) i_r comparison of 3rd and 2nd order models

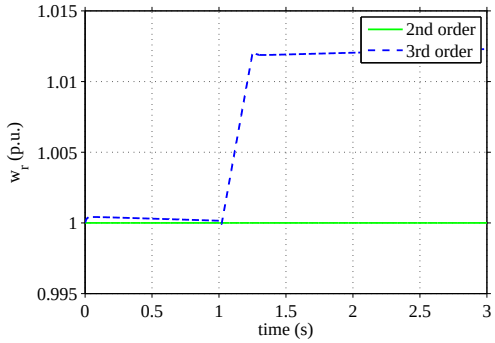

(e) w_r comparison of 3rd and 2nd order models

Figure A.10: Comparison of 3rd and 2nd order models, synchronous operation, 0.25 p.u. voltage dip.

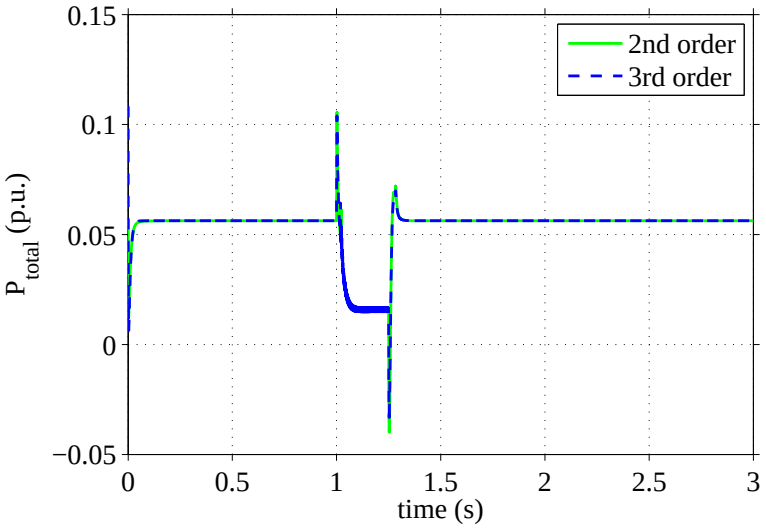

(a) P_{total} comparison of 3rd and 2nd order models

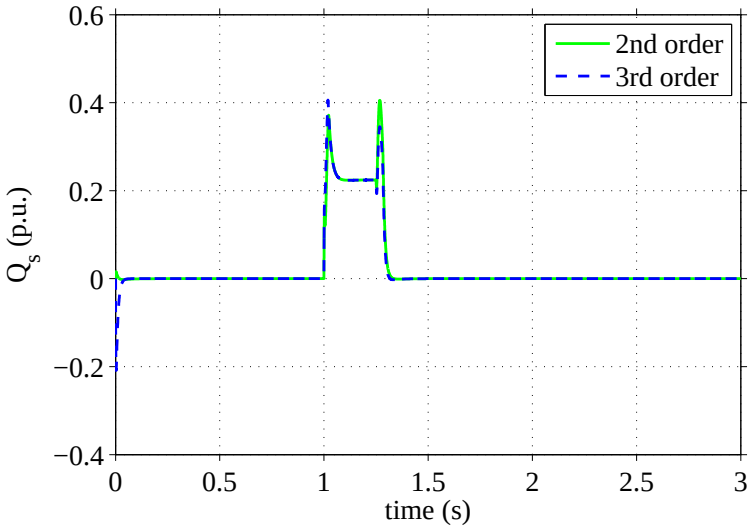

(b) Q_s comparison of 3rd and 2nd order models

Figure A.11: P_{total} and Q_s comparison of 3rd and 2nd order models, sub-synchronous operation, 0.25 p.u. voltage dip.

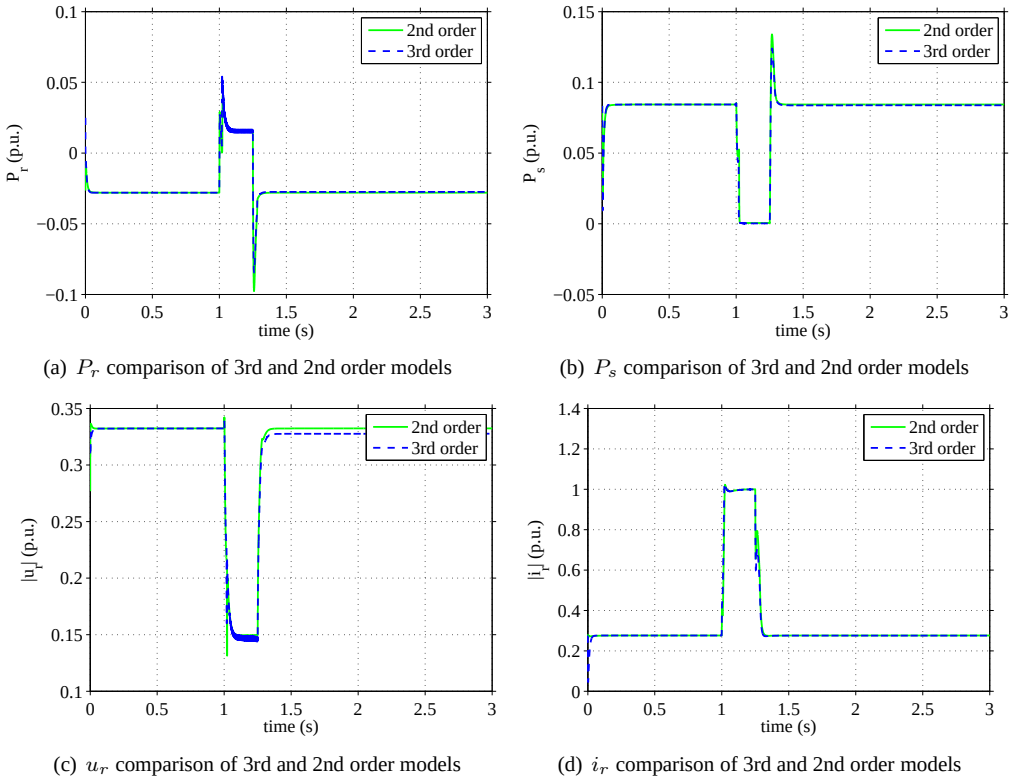

(a) P_r comparison of 3rd and 2nd order models

(b) P_s comparison of 3rd and 2nd order models

(c) u_r comparison of 3rd and 2nd order models

(d) i_r comparison of 3rd and 2nd order models

Figure A.12: Comparison of 3rd and 2nd order models, sub-synchronous operation, 0.25 p.u. voltage dip.

A.3 Comparison of 2nd order model to simplified model

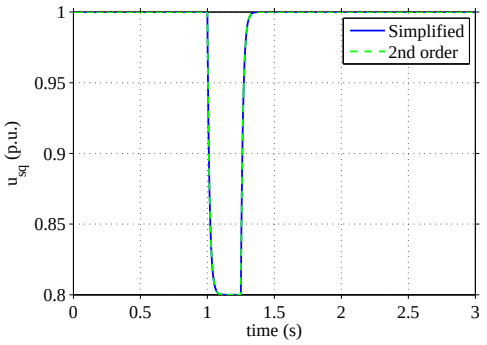

(a) u_s comparison of 2nd order and simplified models

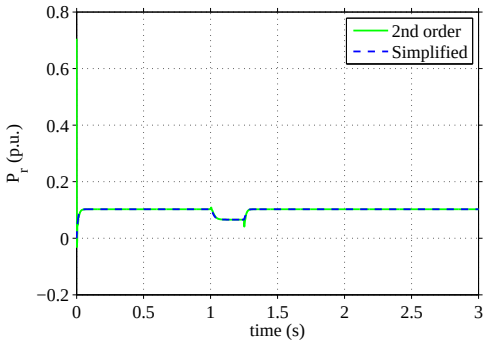

(b) P_r comparison of 2nd order and simplified models

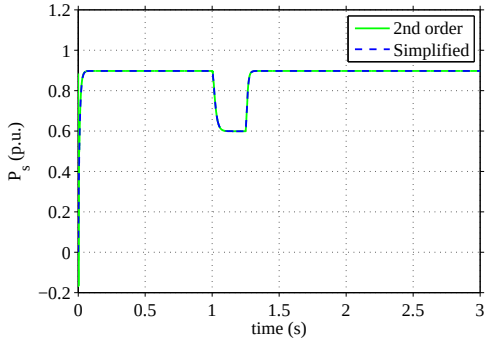

(c) P_s comparison of 2nd order and simplified models

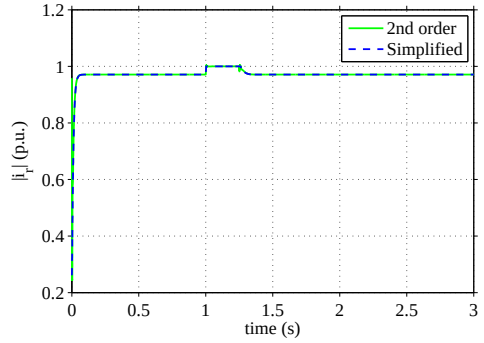

(d) i_r comparison of 2nd order and simplified models

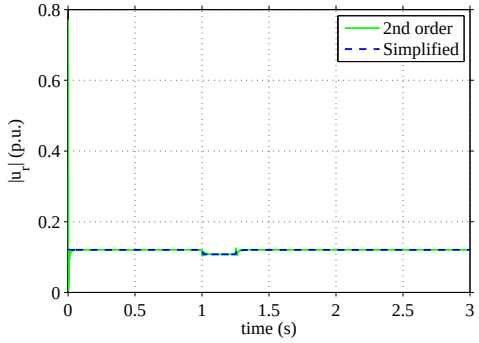

(e) u_r comparison of 2nd order and simplified models

Figure A.13: Comparison of 2nd order and simplified models, super synchronous operation, 0.8 p.u. voltage dip.

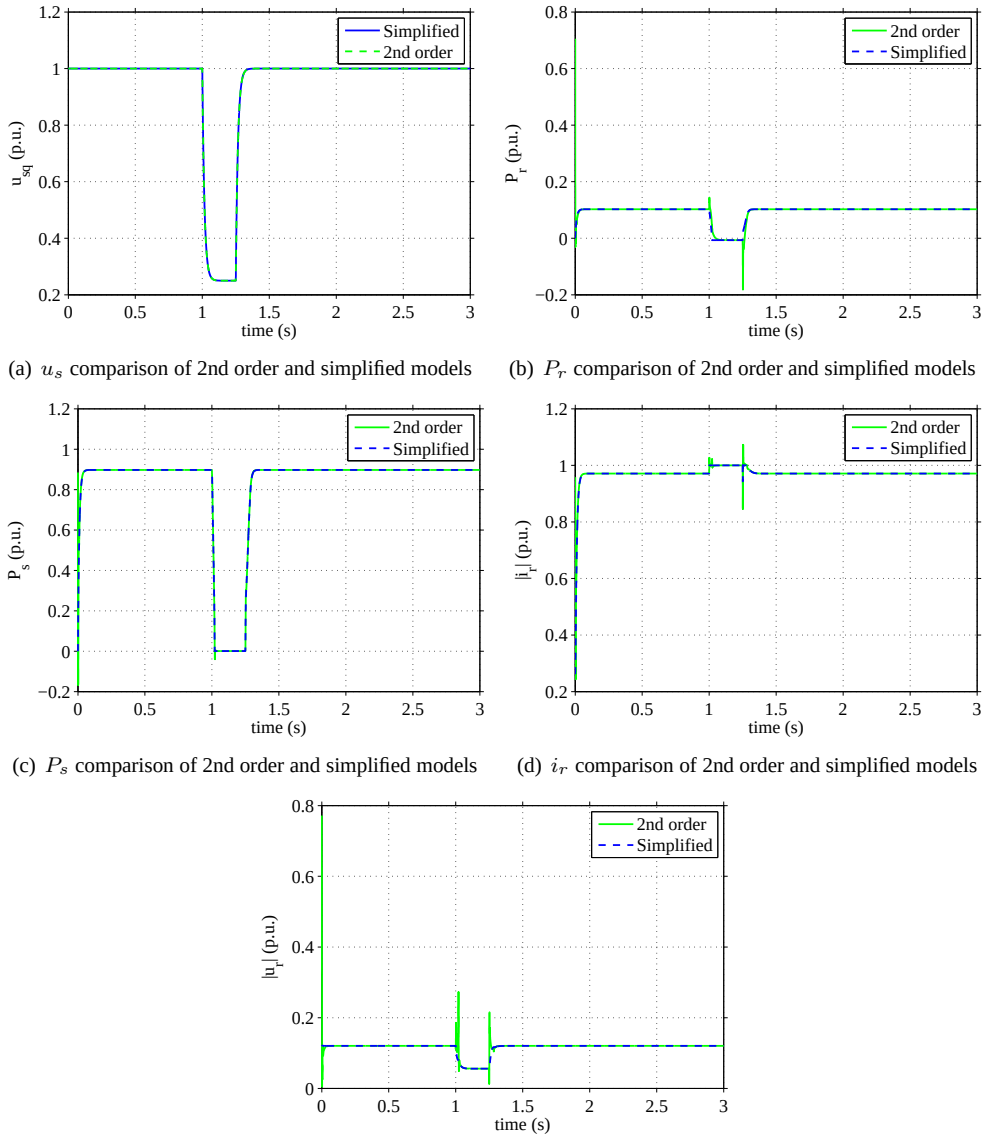

(a) u_s comparison of 2nd order and simplified models

(b) P_r comparison of 2nd order and simplified models

(c) P_s comparison of 2nd order and simplified models

(d) i_r comparison of 2nd order and simplified models

(e) u_r comparison of 2nd order and simplified models

Figure A.14: Comparison of 2nd order and simplified models, super synchronous operation, 0.25 p.u. voltage dip.

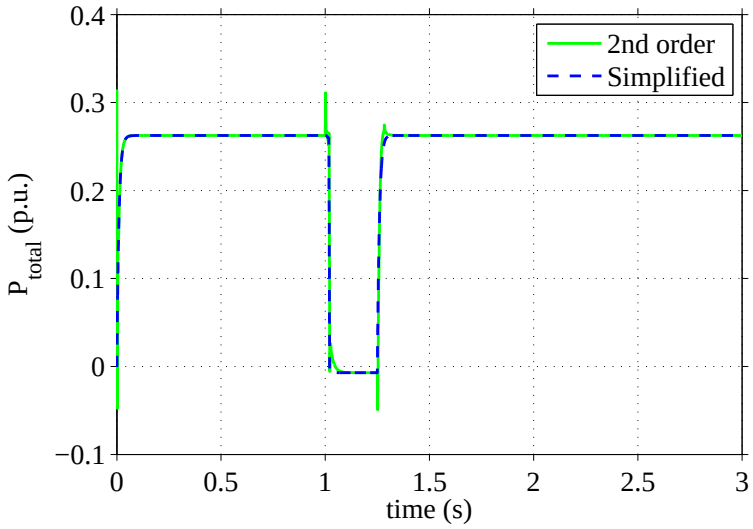

(a) P_{total} comparison of 2nd order and simplified models

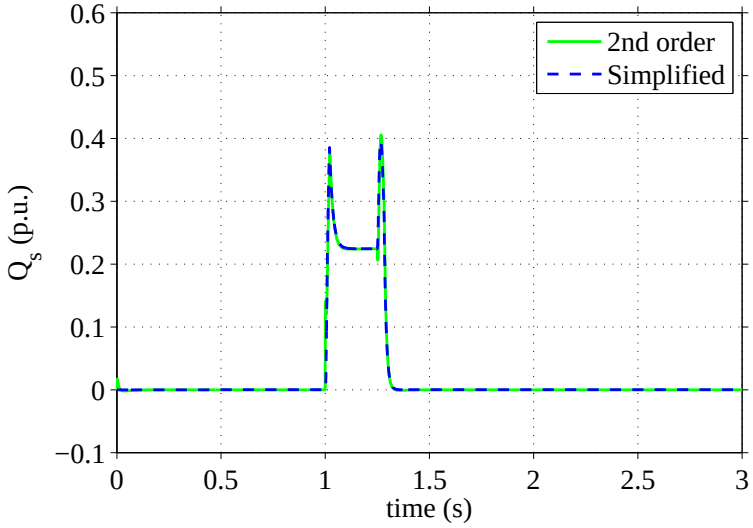

(b) Q_s comparison of 2nd order and simplified models

Figure A.15: P_{total} and Q_s comparison of 2nd order and simplified models, synchronous operation, 0.25 p.u. voltage dip.

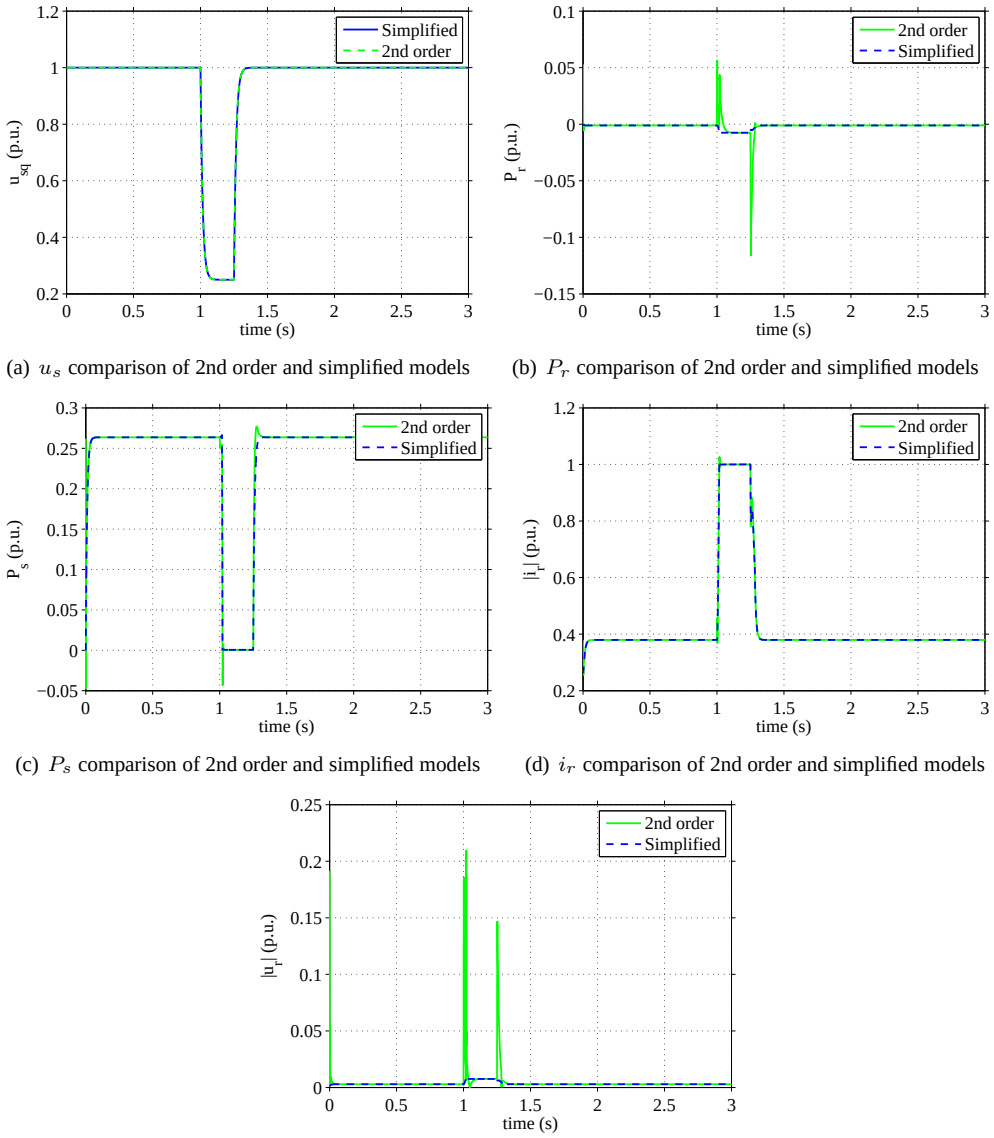

(a) u_s comparison of 2nd order and simplified models

(b) P_r comparison of 2nd order and simplified models

(c) P_s comparison of 2nd order and simplified models

(d) i_r comparison of 2nd order and simplified models

(e) u_r comparison of 2nd order and simplified models

Figure A.16: Comparison of 2nd order and simplified models, synchronous operation, 0.25 p.u. voltage dip.